

FTP IM INN-06/10
UMN-TH-2438/06

Impact of m_{B_s} on the determination of the unitary triangle and bounds on physics beyond the Standard Model

L. Velasco-Sevilla ¹

William I. Fine Theoretical Physics Institute
University of Minnesota

February 18, 2019

Abstract

In this note we study the impact of the recent m_{B_s} results, obtained at the Tevatron Run II by the CDF and D_s collaborations, on the analysis of the Unitary Triangle (UT) in the Standard Model (SM) and in particular show how these measurements further constrain the compatibility between the experimental value of $\sin^{\text{exp}} 2\beta = (0.623; 0.751)$ at 95% C.L. and the value obtained by the fit of the UT parameters considering just CP conserving experimental observables: $\sin^{\text{CP conserv}} 2\beta = (0.751; 0.841)$ at 95% C.L. We also obtain new bounds on certain classes of processes beyond the SM.

¹ liliana@physics.umn.edu

1 Introduction

We are at an exciting era of b -flavoured hadron physics, as the ongoing experimental efforts in this area can be used to test to a better accuracy the CKM matrix and hence the Standard Model (SM) giving at the same time bounds on processes beyond the SM (BSM).

Until now there exists only a bound on the mass difference which characterizes flavour mixing in the $B_s^0 - \bar{B}_s^0$ system, m_{B_s} . However, both experiments operating at the Tevatron Run II, CDF and D_s, are currently pursuing analyses aimed at achieving a first measurement of the parameter m_{B_s} . During the last year indeed they have reported first preliminary results [1] shifting the bound of $m_{B_s} > 14.5 \text{ ps}^{-1}$ up to $m_{B_s} > 16.6 \text{ ps}^{-1}$ and reaching a combined measured sensitivity of 19.6 ps^{-1} , which is the information we use in the present note.

This constitutes already a sizable contribution to the combined oscillation data, which is reported by the Heavy Flavor Averaging Group [1, 2], expressed through the amplitude scan method [10]. Now then this translates not only in the determination of the CKM parameters and its compatibility with each experimental measure, but also in constraining models BSM?

This is the motivation of the present note. The CKM fitter group [3] and the UT group [4] have been developing state of the art analyses and continuously updating the experimental information, however we perform this analysis first at all to study the impact of m_{B_s} on the determination of the unitary triangle (UT) parameters and secondly, with the motivation of having a code compatible with such state of the art analyses in order to test models BSM. To this end we first update the UT fits of the SM comparing the pre-Run II (i.e. the combined oscillation data before CDF and D_s results at Run II were available) and the post-Run II situations, which has not been included in any other analysis so far. Then we begin our tests of models BSM with the Minimal Flavour Violation (MFV) scenario and briefly mention consequences for an example of a horizontal symmetry.

During the last and the present decades many groups have been developing analysis to test the unitary triangle and CP violation using various approaches, the Bayesian method [5], the Range-fit (R-fit) method [6], based on a frequentist approach, a Gaussian method [7], and the scan method [8]. These approaches treat in somewhat different ways the available information on the experimental and the theoretical uncertainties. We use the Bayesian approach to construct a global inference function for the Wolfenstein parameters and, from which a posterior probability density function (pdf) for the all the fitted (within the analysis) and related parameters to the unitary triangle and the constraints used to determine it can be derived.

The analysis of the UT and CP violation tests the SM, hence giving it a more robust successor, if physics BSM is present already at sizable levels, detecting inconsistencies with the various unitary tests.

In what it has been called the Classic analysis of the UT [7], the CP conserving parameters $\{V_{ub}, V_{cb}\}$, m_{B_d} and $m_{B_d} = m_{B_s}$ and CP violating ones $\{V_{cb}, V_{cb}^*, V_{ub}, V_{ub}^*, V_{cb}V_{ub}^*, V_{cb}V_{ub}\}$ are considered. The

$\sin(2\beta)$ are taken into account. The ratio $\mathcal{V}_{ub}/\mathcal{V}_{cb}$ is not expected to have a big contribution from beyond the tree level processes of semi-leptonic decays from which \mathcal{V}_{ub} and \mathcal{V}_{cb} are extracted. The CP asymmetry in $B_s \rightarrow K_s$ could give deviations from measuring not just the SM unitary angle β but β_{BSM} . Over the past years the SM prediction of this quantity using the other UT parameters was consistent with its observed value. But an important result of the present analysis (as well as other recent analyses) is that there is an incompatibility with the input experimental value $\sin^{\text{exp}} 2\beta = (0.623; 0.751)$ at 95% CL, and the output value of the t including just the CP conserving parameters: $\sin^{\text{CP conserv}} 2\beta = (0.751; 0.841)$ at 95% CL, which it is important for it hints BSM processes but of course the actual measurement of m_{B_s} and a better determination of the parameters \mathcal{V}_{ub} and \mathcal{V}_{cb} will be needed in order to resolve this incompatibility. We just consider $F = 2$ flavour changing processes, leaving out of our analysis $F = 1$ processes, which although they are relevant in some cases the present experimental bounds are not at the level of precision [11] as are most part of the quantities entering in the classic analysis.

Fixing in the K and the $B_{d,s}$ neutral meson system, from which, m_{B_d} and $m_{B_s} = m_{B_d}$ are respectively obtained, can be particularly sensitive to physics BSM. The most general way to identify the deviation of m_{B_d} and m_{B_s} from their SM prediction it is by measuring the deviation from unity of the ratios

$$\begin{aligned} \text{Im } f_{K^0} \mathcal{H}_{\text{eff}}^{\text{Total}} \mathcal{K}^0 \text{ig} &= \text{Im } f_{K^0} \mathcal{H}_{\text{eff}}^{\text{SM}} \mathcal{K}^0 \text{ig and} \\ h_{B_{d,s}} \mathcal{H}_{\text{eff}}^{\text{Total}} \overline{B}_{d,s}^0 i &= B_{d,s} \mathcal{H}_{\text{eff}}^{\text{SM}} \overline{B}_{d,s}^0 i; \end{aligned}$$

respectively, where $\mathcal{H}_{\text{eff}}^{\text{Total}}$ is the Hamiltonian that takes into account all the processes, both in the SM and BSM of the relevant $F = 2$ ($K^0 \rightarrow K^0$ and $B_{d,s}^0 \rightarrow \overline{B}_{d,s}^0$) flavour changing neutral current processes.

However, we have to bear in mind that there are two main restrictions on measuring these ratios. The first one is that there are still big uncertainties in some quantities entering in the effective SM Hamiltonians, like B_K and $f_{B_d}^2 B_{B_d}$, which obscures differentiation of these and the effects of processes BSM. The second one is that in general these ratios are related in different extensions of models BSM and just for the minimal flavour violation (MFV) scenario of the Minimal Supersymmetric Standard Model (MSSM) the form of the effective Hamiltonians and the QCD next to leading order (NLO) determination of its parameters has been computed [28].

For the first of the aforementioned restrictions not much can be done currently but for the second one we can test models for which we can extract meaningful information from the current way in which the UT analysis it is performed and since we want to test what is the impact of the new results on m_{B_s} we explore the cases of physics BSM for which the ratio $m_{B_d} = m_{B_s}$ is equal to the case of the SM. The MFV violation scenario, which essentially requires that all flavour and CP violating interactions are linked to the known Yukawa couplings, is a well known example of this condition. The MFV scenario can be easily implemented in the MSSM, as it has been done extensively since the pioneering work of [12], but using an effective operator approach [13] it can also be implemented for other cases.

Given the new experimental information we thus study the possibility of having significant contributions of processes beyond the SM in the determination of the CKM elements, and we show that, under certain constraints, somewhat large effects of processes beyond the SM are still possible. We mention briefly the consequences of this analysis for a model of fermion masses with an SU(3) horizontal (flavour) symmetry.

2 Constraints of the CKM matrix

Here we just quickly state the formulas used in the SM fit of the CKM matrix, V , and remark the processes from which they are extracted in order to point out which constraints we use to put bounds on processes beyond the SM. The inputs of the fits are presented in Tables (2)–(3) of the Appendix A. We recall here that V can be expressed in terms of the four Wolfenstein parameters: A , ρ and η . All elements of V can be obtained as a perturbative expansion of ρ up to the desired n -th order, using the unitary condition from the basic definitions

$$|V_{us}| = 1; \quad |V_{cb}| = A^{-2}; \quad |V_{ub}| = A^{-3}(\rho + i\eta); \quad (1)$$

which are valid to all orders in ρ . The parameters ρ and A are obtained from tree level K and B semileptonic decays which have large branching ratios making their determination independent, to an excellent approximation, of any processes beyond the SM.

The parameters $\rho = (1 - \eta^2)^{1/2}$ and $A = (1 - \eta^2)^{1/3}$ are the coordinates of the apex of the unitary triangle (UT), with sides R_b and R_t defined by

$$R_b^2 = \rho^2 + \eta^2; \quad R_t^2 = (1 - \eta^2)^2 + \rho^2 \quad (2)$$

and angles α , β and γ defined by

$$\sin \alpha = \frac{\eta}{R_t}; \quad \sin \beta = \frac{\rho}{R_b}; \quad \gamma = \dots \quad (3)$$

In the classic fit of the SM CKM matrix, α and β are extracted from

(i) CP conserving processes: $\bar{B}_d \rightarrow \bar{D}_s \ell \bar{\nu}_\ell$ & (ii) CP conserving processes: $\bar{B}_d \rightarrow \bar{D}_s \ell \bar{\nu}_\ell$

$$\frac{|V_{ub}|}{|V_{cb}|}, \quad m_{B_d} \text{ and } \frac{m_{B_d}}{m_{B_s}} \quad \text{and} \quad \rho, \quad \eta \quad \text{and} \quad \sin 2\beta.$$

In (i), $|V_{ub}|$ and $|V_{cb}|$ are extracted from the charmless channel of semileptonic decays of B mesons. The parameters m_{B_d} and m_{B_s} are extracted from measurements of $B_{d,s}^0$ oscillations, which are $B = 2$ flavour changing neutral current processes (FCNC). From (ii) the asymmetry parameter ρ_K is extracted from $K^0 \rightarrow \bar{K}^0$ oscillations, which are $S = 2$ FCNC processes. Finally the measurement of $\sin(2\beta)$ is dominated by the channel $B_s^0 \rightarrow K_s^0 \ell \bar{\nu}_\ell$ and complemented by other B decay modes.

The parameters ρ_K , $|V_{ub}| = |V_{cb}|$, m_{B_d} , m_{B_s} and $\sin 2\beta$, are expressed directly or indirectly in terms of α and β and a set of theoretical and experimental parameters

x , some of which have been well measured and some of them have still dominant uncertainties. Thus in the fits the parameters x 's which have been well measured are kept fixed and those with dominant uncertainties are varied and fitted as well.

$$|V_{ub}|/|V_{cb}|$$

The CKM matrix elements $|V_{ub}|$ and $|V_{cb}|$ are measured in exclusive and inclusive charm-less semileptonic B decays. In terms of the re-scaled Wolfenstein parameters, $|V_{ub}|/|V_{cb}|$ is expressed as:

$$\frac{|V_{ub}|}{|V_{cb}|} = \frac{q}{c} \frac{\overline{c}^2 + \overline{s}^2}{\overline{s}^2} : \quad (4)$$

m_{B_d} and m_{B_s}

Within the SM, the mass differences of the oscillating systems $B_{d;s}^0 - \overline{B}_{d;s}^0$, $m_{d;s}$ are very well approximated by the relevant electroweak transition ("box") diagrams, described by the Inami-Lim functions [14], which are dominated by top-quark exchange. $m_{B_{d;s}}$ are proportional to the effective Hamiltonian for the $B = 2$ transitions

$$m_{B_q} = \frac{G_F^2}{6^2} m_{B_q} f_{B_q}^2 B_{B_q} B_S(x_t) |V_{tb}|^2 / |V_{cb}|^2 H_{\text{eff}}^{\text{SM}} \mathcal{B}_q i \gamma^5 \quad (q = d; s) \quad (5)$$

where G_F is the Fermi constant, B is a QCD correction factor calculated in NLO, m_{B_q} and m_W are the B_q meson and W boson masses respectively. The dominant uncertainties in equation Eq. (5) come from the evaluation of the hadronic quantities: f_{B_q} , the B meson decay constant, and B_{B_q} , which parameterizes the value of the hadronic matrix element. The Inami-Lim function, $S(x_t)$, describes the $|B| = 2$ transition amplitude in the absence of strong interaction, where the mass of the top quark enters via $x_t = \frac{m_t^2}{M_W^2} \cdot 2$.

In terms of the Wolfenstein parameters, Eq. (5) above, for the B_d case can be expressed as

$$m_{B_d} = C_m A^{2/6} [(1 - \overline{c}^2)^2 + \overline{s}^2] m_{B_d} f_{B_d}^2 B_{B_d} B_S(x_t); \quad (6)$$

where we have defined the constant $C_m = \frac{G_F^2 M_W^2}{6^2}$. The parameters with dominant uncertainties in equation (6) are $f_{B_d}^2 B_{B_d}$; A and \overline{c} , which are varied parameters of the fit. The size of side $|V_{td}|/|V_{cb}|$ of the unitary triangle can be obtained from the ratio of $|m_{B_d}|$ and $|m_{B_s}|$:

$$\frac{m_{B_d}}{m_{B_s}} = \frac{m_{B_s} |V_{td}|^2}{m_{B_s}^2 |V_{ts}|^2} ; \quad = \frac{f_{B_s}^2 B_{B_s}}{f_{B_d}^2 B_{B_d}} ; \quad (7)$$

$$^2 S(x_t) = x_t \left(\frac{1}{4} + \frac{9}{4} \frac{1}{1-x_t} - \frac{3}{2} \frac{1}{(1-x_t)^2} \right) \left(\frac{3}{2} \frac{1-x_t}{1-x_t} \right)^{i_3} \ln x_t ;$$

which is expected to be less dependent on the absolute values of f_B and B_B and hence it can be characterized by $\frac{P}{f_B B_B}$, whose value is obtained from lattice QCD calculations. We use $\frac{P}{f_B B_B}$ instead of $f_{B_d} B_{B_d}$, which makes the constraint m_{B_d} more effective [38]. The constraint we use from m_{B_s} is expressed, from equation (7), as

$$m_{B_s} = m_{B_d} \frac{m_{B_s}}{m_{B_d}} 2 \frac{C^2}{2} \frac{1}{(1 - \gamma^2)^2}; \quad (8)$$

where m_{B_d} is here taken as an experimental input. The parameters with dominant uncertainties in equation (8) are γ ; A ; C , which are varied parameters of the fit.

$$j_K j$$

The parameter $j_K j$ expresses the measurement of indirect CP violation in the neutral K system. In terms of the Wolfenstein parameters it is given by

$$\begin{aligned} j_K j &= C B_K \text{Im } A_{SM}(K) / h K_0 H_{eff}^{SM} K_0 i \\ \text{Im } A_{SM}(K) &= A^{2/6} [\alpha x_c + A^{2/4} (1 - \gamma) \bar{t} S(x_t) + \bar{c} t S(x_c; x_t)]; \\ C &= \frac{G_F^2 f_K^2 m_K m_W^2}{6^{2/2} m_K}; \end{aligned} \quad (9)$$

The short distance QCD corrections are coded in the coefficients α , \bar{t} and $\bar{c} t$, and are functions of the charm and top quark masses and of the QCD scale parameter Q_{CD} ; these parameters have been calculated in the NLO. The Inami-Lim functions, which describe the $j_S j=2$ transition amplitude in the absence of strong interactions, are given by $S(x_t)$, as in the m_{B_d} case², and by $S(x_c; x_t)$.³ The parameters with dominant uncertainties are B_K , α , $\bar{c} t$, m_c and m_t and hence these are varied in the fit.

$$\sin 2$$

A direct determination of the angles of the unitary triangle can be achieved via measurements of CP asymmetries in various B decays. These angles are defined in reference to the normalized unitary triangle:

$$\begin{aligned} \theta &= \arg \frac{V_{td} V_{tb}^*}{V_{ud} V_{ub}^*}; \quad \phi = \arg \frac{V_{cd} V_{cb}^*}{V_{td} V_{tb}^*}; \quad \gamma = \arg \frac{V_{ud} V_{ub}^*}{V_{cd} V_{cb}^*}; \end{aligned} \quad (10)$$

The value of $\sin 2\gamma$ is measured in $b \rightarrow cc$ decays such as $B \rightarrow J/\psi K^0$. The UT angles can be expressed directly in terms of the re-scaled Wolfenstein parameters, giving:

$$\sin 2\gamma = \frac{2 \gamma}{2 + (1 - \gamma)^2} \quad (11)$$

³ $S(x_c; x_t) = x_c \ln x_c + x_c \frac{\ln \frac{x_t^2 - 8x_t + 4}{4(1 - x_t)^2}}{\frac{x_t^2 - 8x_t + 4}{4(1 - x_t)^2}} \ln x_t + \frac{3}{4} \frac{x_t}{x_t - 1}; \quad x_q = \frac{m_q^2}{M_W^2};$

3 How to account for indications of physics beyond the SM

The ratio $\mathcal{Y}_{ub}/\mathcal{Y}_{cb}$ is not expected to have a big contribution from beyond tree level processes of semi-leptonic decays from which \mathcal{Y}_{ub} and \mathcal{Y}_{cb} are extracted. Mixing in the K and $B_{d,s}$ systems however can be particularly sensitive to physics beyond the SM (BSM). In general their deviation from the SM can be expressed by

$$\begin{aligned} r_{B_{d,s}} e^{2 \beta_{B_{d,s}}} &= \frac{h B_{d,s} \mathcal{H}_{eff}^{Total} \beta_{B_{d,s}}}{h B_{d,s} \mathcal{H}_{eff}^{SM} \beta_{B_{d,s}}} ; \\ r_K &= \frac{\text{Im } f h K_0 \mathcal{H}_{eff}^{Total} \mathcal{K}_0 i g}{\text{Im } f h K_0 \mathcal{H}_{eff}^{SM} \mathcal{K}_0 i g} \end{aligned} \quad (12)$$

where new CP phases may arise as a result from the interference between mixing and decay amplitudes in the $B_{d,s}$ systems. Thus CP violating asymmetries would involve not only \mathcal{Y}_{ub} and \mathcal{Y}_{cb} but additionally β_{B_d} and β_{B_s} :

$$\sin 2 \beta = \sin(2 \beta_{B_d}^{SM} + 2 \beta_{B_s}) ; \quad \beta = \beta_{B_d}^{SM} \quad (13)$$

where the parameters of the B_s system are not included and cannot be determined at the moment since m_{B_s} and $A_{CP}(B_s)$ are not yet measured. For the K system, m_K is not considered due to the lack of control in the QCD long distance effects in the $K^0 \bar{K}^0$ system and hence a possible additional phase BSM in this sector is neglected. In general the BSM contributions to the real parts of m_{B_d} , m_{B_s} and β_K are no longer proportional to the CKM matrix elements as in the SM

$$\begin{aligned} h B_q \mathcal{H}_{eff}^{SM} \beta_q i &/ V_{tq} V_{tb} ; \quad (q = d, s) \\ h K_0 \mathcal{H}_{eff}^{SM} \mathcal{K}_0 i &/ (V_{cd} V_{cs})^2 ; (V_{td} V_{ts})^2 ; (V_{cd} V_{cs}) (V_{td} V_{ts}) ; \end{aligned} \quad (14)$$

but in the best case they will only have additional contributions to them. This is the point that can be used if we want to extract useful information of processes BSM from the analysis of the Unitary Triangle. Meaningful bounds on such processes can be extracted from $B_{d,s}^0 \bar{B}_{d,s}^0$ and $K^0 \bar{K}^0$ whenever the corresponding effective Hamiltonians are still proportional to the combination of CKM elements as given in Eq. (14) and such that there is only a change in the contribution to the box diagrams of these $F = 2$ transitions. This amounts to a replacement of $\mathcal{S}(x_t)$ in β_K , as appears in Eq. (9) and as a replacement of $B_S(x_t)$ in m_{B_d} and m_{B_s} , as appear in Eq. (5), by new functions describing the contribution of particles BSM, which can be generically be written as

$$\begin{aligned} m_{B_d} &= \frac{G_F^2 M_W^2}{2^2} m_{B_d} f_{B_d}^2 \hat{B}_{B_d} \mathcal{Y}_{td} V_{tb} \mathcal{J}_B \mathcal{S}(x_t) + S_{m_{B_d}} \text{ and} \\ \mathcal{J}_K \mathcal{J} &= C B_K A^{2/6} \mathcal{J}_{cc} x_c + \mathcal{J}_{ct} S(x_c; x_t) + A^{2/4} (1 - \mathcal{J}_{tt}) \mathcal{S}(x_t) + S_K \mathcal{J} ; \end{aligned} \quad (15)$$

respectively, by normalizing the QCD correction factors of the processes BSM with respect to those of the SM.

The set of theories which satisfy these conditions is quite restrictive, but it is important to note that the bounds put on them are at the same level of precision at which the SM unitary triangle parameters can be currently determined. On the other hand we cannot test by these means new exciting theories for which there are contributions to box and penguin diagrams that are not proportional to the CKM matrix elements as the SM top contribution, or there are complex phases beyond the phases of the CKM or new local operators (contributing to the relevant amplitudes) and hence introducing additional non-perturbative factors B_i and box and penguin diagrams.

4 Statistical analysis of the unitary triangle

4.1 Likelihood technique

We include this section mainly for the sake of completeness, since this technique has been well documented [15], and because we refer to it in the following sections. The likelihood technique for the analysis of the unitary triangle (UT) in the SM has been widely studied. The Bayesian approach has been investigated by the UT Fitter group [4]. We have followed such approach in implementing our code with emphasis on the importance of the increasing knowledge of m_s .

In the Bayesian approach, the combined probability distribution for θ and m_s is identified with the likelihood

$$L(\theta, m_s) \propto \prod_{j=1}^M f(c_j | \theta, m_s) \prod_{i=1}^N f_i(x_i) dx_i f_0(\theta); \quad (16)$$

where $f(c_j | \theta, m_s)$ is the conditional probability density function (pdf) of the constraints $c_j = \frac{V_{ub}}{V_{cb}} \frac{m_{B_d}}{m_{B_s}}$, $m_{B_d} = m_{B_s}$, K and $\sin 2\beta$, given their dependence as functions of the SM parameters, θ , m_s , A , and x_i . Besides the constraints themselves, there are two classes of involved parameters: (i) fitted, with pdf $f_i(x_i)$, (e.g. the top mass); and (ii) fixed, which are taken as constant (e.g. the W mass).

The prior probability density functions $f(c_j)$ for the constraints are considered to be Gaussian distributions, except for m_{B_s} , for which a direct measurement is not yet available.

The pdf used, in order to be consistent with the Bayesian approach, is implemented via the likelihood ratio, R , after accessing the amplitude point $(A; \theta_A)$ associated to the frequency value obtained by evaluating the r.h.s. of Eq. (8).

For $f_i(x_i)$ we consider Gaussian and in some cases flat probabilities. A Gaussian pdf is chosen when the uncertainty is dominated by statistical effects, or there are many contributions to the systematics error, so that the central limit theorem applies. Otherwise, a flat (uniform) distribution is used for the uncertainty. When both a Gaussian and a flat uncertainty components are available for a parameter, the resulting pdf is obtained by convoluting the two distributions. I.e., for an observable parameter

x of true value x , with Gaussian and uniform uncertainty components, g , u , one has for the parameter and its pdf, $f(x)$,

$$x = x + x_g + x_u \quad ! \quad f(x) = (x - x) \text{Gaus}(x_j_g) \text{Unif}(x_j_f);$$

The integration of Eq. (16) can be performed using Monte Carlo methods and then normalized. Hence we can calculate all the pdfs for the parameters involved in the fit. The expression Eq. (16) shows explicitly that whereas a priori all values of x and g are equally likely by assumption, i.e. $f_0(\cdot) = \text{const.}$, a posteriori the probability clusters in a region of maximum likelihood.

The probability regions in the (\cdot, \cdot) plane are constructed from the pdf obtained in Eq. (16). These are called highest posterior density regions, and are defined such that $L(\cdot, \cdot)$ is higher everywhere inside the region than outside,

$$P_w = \int_{\mathbb{R}} L(z) dz = w; L(z^0) < m \text{ in}_{P_w} L(z); 8_{z^0 \in P_w} g.$$

The one dimensional pdfs are obtained similarly. For example, the x pdf is obtained as $L(\cdot) / \int_{\mathbb{R}} L(\cdot) dz$, from which its expected value can be calculated together with the corresponding highest posterior density intervals.

A similar procedure can be in principle used in order to obtain the pdf for other desired parameters. Technically, one may also use the probability function for transformed variables; i.e., that for $u(x)$ one has $f(u) = f(x) \frac{\partial x}{\partial u} j$ where the last factor denotes the Jacobian. In this way, the pdf for a parameter x can be obtained from

$$L(x) / \int_{\mathbb{R}} L(x; \cdot) dz / \int_{\mathbb{R}} L(\cdot) \frac{d}{dx} dz; \quad (17)$$

where $L(\cdot, \cdot)$ has been computed in Eq. (16) above.

Besides the probability distribution in the (\cdot, \cdot) plane, we are most interested in obtaining the posterior probability distribution for the m_{B_s} parameter.

5 Using the available B_s flavour oscillation results

5.1 Experiments { short overview

The study of oscillations in the $B_s^0 \{ B_s^0$ system has been the subject of many past experimental analyses, performed at ALEPH, CDF, DELPHI, OPAL and SLD. A wide range of data analysis techniques has been employed, which have been developed for taking advantage of detector capabilities and the characteristics of the collected data samples. These involve from fully exclusive, where the B_s decays are completely reconstructed, to fully inclusive methods, which aim at identifying the mesons decay vertices; along with several b-flavour tagging techniques. The most sensitive among these analyses were those based on semi-exclusive or semi-inclusive lepton samples, where the D_s , resulting from the semi-leptonic B_s decay, was either inclusively or exclusively reconstructed.

In general, the more inclusive analyses benefit from considerably larger number of candidates, while the more exclusive ones take advantage of the more precise information about the decay candidates which is available. In practice, therefore, the resulting

sensitivity to B oscillations is dependent on a trade-off between the quantity and the quality of the events forming the samples. Furthermore, the relative weight of the latter increases quickly when probing higher oscillation frequencies. Accordingly, the significance of an oscillation signal at relatively lower frequencies benefits more readily from high statistics samples, provided the events are characterized by sufficiently adequate resolutions. This has to some extent been the case until now. The situation becomes different for a signal of a higher frequency, which is indeed expected to be the case for the B_s system | a measurement of m_{B_s} will therefore require samples with very good resolutions together with adequately large yields.

A new generation of B_s mixing analysis is being undertaken by the CDF and D collaborations, which are accumulating large samples of B_s meson decays produced in the p-p collisions of the Tevatron at Fermilab. Both collaborations reported their first preliminary results during the past year. These involve samples of both partially reconstructed semi-leptonic $B_s \rightarrow D_s 1^-$ decays and fully reconstructed $B_s \rightarrow D_s(3)$ decays, with the D_s meson being reconstructed in several exclusive channels. The sensitivity is so far dominated by the semi-exclusive analyses, characterized by larger statistics, while the exclusive samples, with precise momentum resolutions, provide the leading contributions for the large probed frequencies. These results have already a considerable impact on the combined world results [1]. The increasing size of the data samples which will continue to be accumulated together with the use of improved and additional analysis techniques which are being developed by the collaborations may result in exciting updates to the already announced results. It is expected that a combined sensitivity above the SM most favoured region is within reach at Run II.

Following the Tevatron the excitement of the study of the B_s system will be transferred to the LHC experiments: the LHCb, as well as the general purpose detectors ATLAS and CMS. At the LHCb alone, and within a single year of data taking, a large enough sample of $B_s \rightarrow D_s$ modes is expected to be gathered which will allow a measurement far beyond the SM prediction.

Regardless of how soon a first direct measurement is achieved, the recent results and expected updates are already quite exciting. It is interesting to investigate how these impact on the t to the constraints on the CKM triangle and on the evaluation of the resulting effects on bounds to BSM scenarios.

5.2 Measurements { amplitude scan

The study of oscillations is based on the analysis of the proper decay time of the B_s candidates. It involves in general the measurement of the B meson decay distance and momentum, as well as a determination of whether a change of its flavour, $B \rightarrow B$ or vice-versa, has occurred.

The model used to describe the proper time distribution involves the exponential decay dictated by the system's lifetime, modulated by an oscillating term describing

the probability for the B_s to have mixed,

$$P(t) = \frac{1}{2} \exp^{-\frac{t}{A}} (1 - A \cos m_{B_s} t) : \quad (18)$$

This expression needs to be adapted to take into account detector resolutions, reconstruction effects, and imperfections of the b-flavour tagging methods employed.

The parameter A has been introduced in Eq. 18 in an ad-hoc fashion for implementing the so-called amplitude method [10]. Instead of extracting from the data the quantity of interest $\{m_{B_s}\}$ directly, in this method the likelihood is maximized as a function of A , while m_{B_s} is a fixed parameter of the fit. The procedure is repeated for any different values of m_{B_s} , and the result is thus conveyed as a set of measured $A(m_{B_s})$ and $\chi^2(m_{B_s})$ in a spectrum of probed oscillation frequencies. The value of A should fluctuate around zero unless the true oscillation frequency of the system is being probed, for which case A should be consistent with unity, within its errors. A given frequency value is thus excluded at 95% CL if the corresponding amplitude and its uncertainty satisfy $A + 1.645 \Delta_A < 1$; the lower exclusion limit of an experiment is defined as the m_{B_s} value below which all frequencies satisfy the latter condition. The sensitivity of an analysis is defined as the largest frequency for which $1.645 \Delta_A < 1$ holds; i.e. it is the largest excluded frequency if A were exactly zero as it's expected in the absence of a signal, removing the dependence on fluctuations of the central value A which affects limits.

The amplitude method was originally introduced in [10] as a convenient approach to set limits, as well as for combining such exclusion regions obtained with different analysis. It has provided a consistent fitting procedure through which all experiments have expressed their results, the combination of these being done straightforwardly as standard averages of Gaussian measurements. In the averages performed by HFAG [9] the measurements are further adjusted on the basis of common physics input values, and possible statistical correlations are taken into account. The world-average exclusion limit and sensitivity were 14.5 ps^{-1} and 18.2 ps^{-1} , respectively, before including the Run II results; while with the Tevatron recent results (2005) these become 16.6 ps^{-1} and 19.6 ps^{-1} , respectively.

5.3 Likelihood implementation

The 95% CL exclusion limit and the sensitivity at which it is achieved provide a rather concise way of summarizing the results of the analysis.

However, in our fit to the CKM parameters we ought to use the more complete information which is provided by the full amplitude scan.

The measured values of the amplitude and its uncertainty, A and Δ_A , may be used to derive [10], in the Gaussian approximation, the log-likelihood function, $\ln L^{-1}(m_{B_s})$, referenced to its value for an infinite oscillation frequency

$$\ln L^{-1}(m_{B_s}) = \ln L(1) - \ln L(m_{B_s}) = \frac{1}{2} \Delta_A - \frac{1}{2} \frac{1}{\Delta_A};$$

$$\ln L^1 (m_{B_s})_{\text{mix}} = \frac{1}{2} \frac{1}{A};$$

$$\ln L^1 (m_{B_s})_{\text{nomix}} = + \frac{1}{2} \frac{1}{A};$$

The last two relations give the expected average log-likelihood value for the cases when m_{B_s} corresponds to the true (mixing case) or is far from (no-mixing case) oscillation frequency of the system, characterized respectively by unit and null expected amplitude values. These are shown in Figure (1-a).

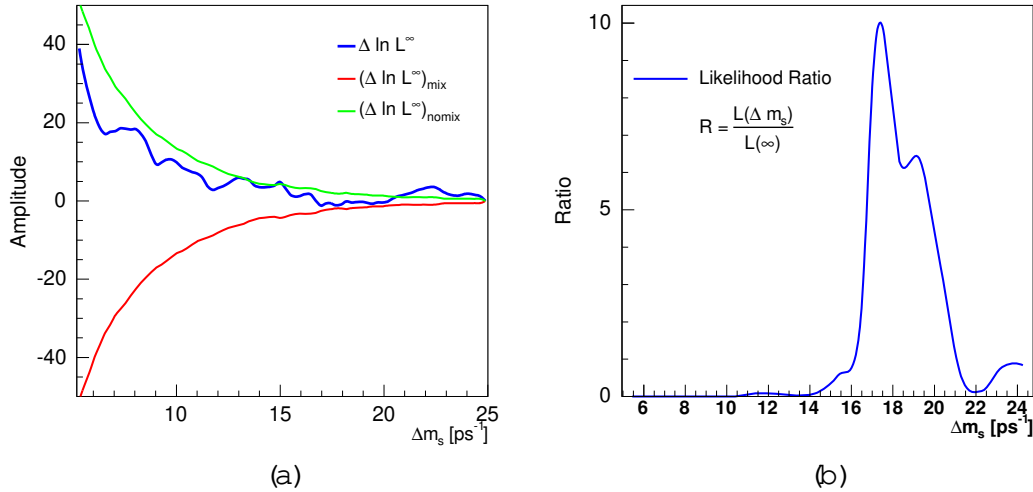


Figure 1: Likelihood for m_{B_s} obtained from the combined amplitude measurements, including Tevatron's Run II.

The log-likelihood difference, according to the central limit theorem of likelihood theory is χ^2 -distributed: $\ln L = \frac{1}{2} \chi^2$. We translate therefore the amplitude scan into the likelihood ratio

$$R(m_{B_s}) = e^{-\ln L^1(m_{B_s})} = \frac{L(m_{B_s})}{L(1)} = e^{\frac{1}{2} \frac{A(m_{B_s})}{A(1)} - \frac{1}{2}}; \quad (19)$$

through which the constraint for m_{B_s} is implemented in the fit. This is represented in Figure (1-b). We re-iterate that the exponent in Eq. (19) corresponds to the χ^2 , or log-likelihood, difference between the cases where an oscillation signal is present and absent, for which the true amplitude value is 1 and 0, respectively: $\frac{1}{2} \frac{A(1)}{A(0)} - \frac{1}{2}$. Note that hypotheses for m_{B_s} associated with larger and more precisely measured A -values in the scan contribute a larger weight in the fit.

5.4 Extending the amplitude spectrum

The amplitude fits are performed for m_{B_s} values lower than a given threshold, beyond which the fit behavior may become unstable. On the other hand, in the framework of

the CKM t , it is in principle desirable to have R defined for all positive frequency values, which in turn demands for a continuation of the amplitude spectrum beyond what is measured.

The extrapolation of the value of A may be achieved, under the assumption of absence of a true oscillation signal in that region of the spectrum, through an analytical description [10] of the measured significance curve

$$A / e^{\frac{1}{2} \frac{t}{\tau} m_{B_s}^2};$$

where t denotes the uncertainty in the measured proper decay time (this expression would in fact need to be properly averaged over the samples signal uncertainty distributions).

An extrapolation of A itself as such is not possible, however it is here sufficient to note that its expected values lie in the vicinity of either zero or unity as already mentioned. Therefore, for the unmeasured part of the spectrum, the exponent in Eq. (19) becomes small, and quickly approaches zero. We take this asymptotic limit as the criterion for extending R beyond the experimentally probed frequencies.

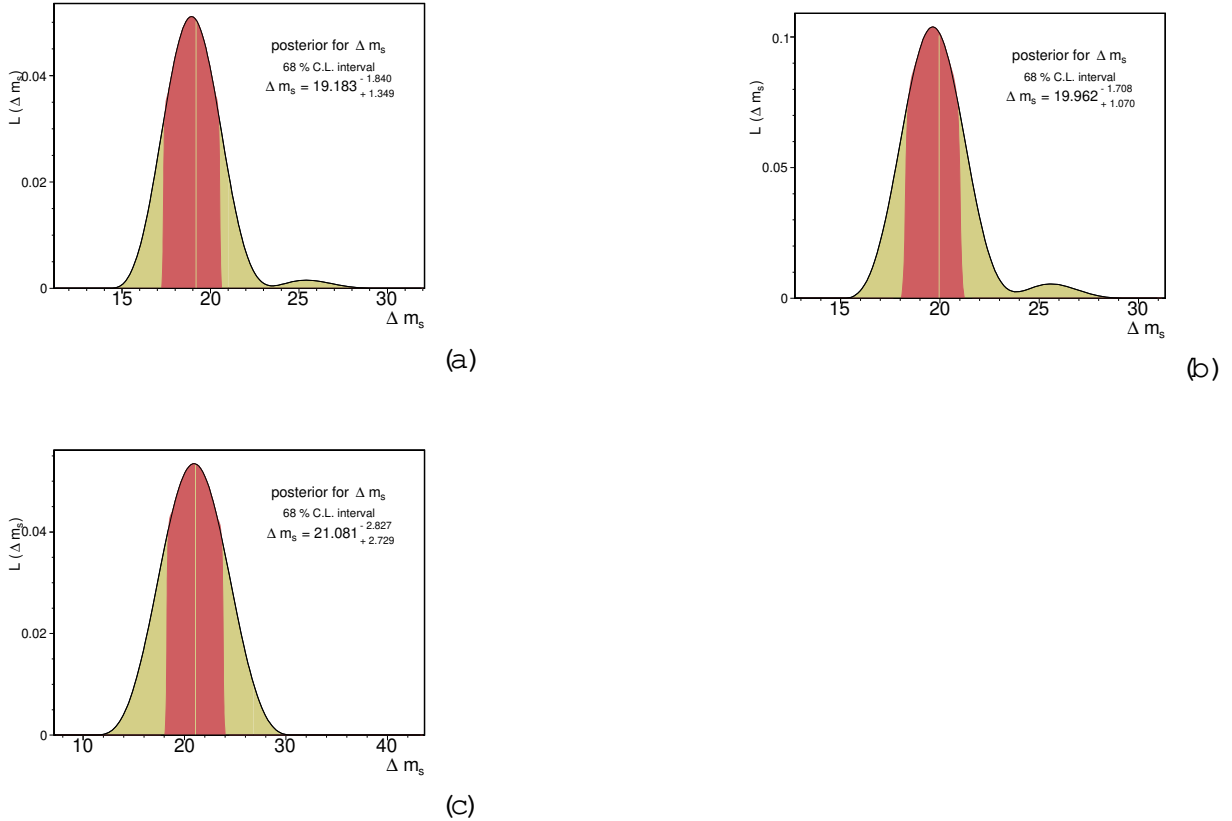


Figure 2: Probability density function of m_{B_s} as a result of the unitary triangle t using the (a) pre-Run II and (b) the t using post-Run II data. In figure (c) it shown the output of m_{B_s} without using this constraint in the t .

6 Tests of the SM in the UT analysis

6.1 Classic Fit pre-Run II and post-Run II

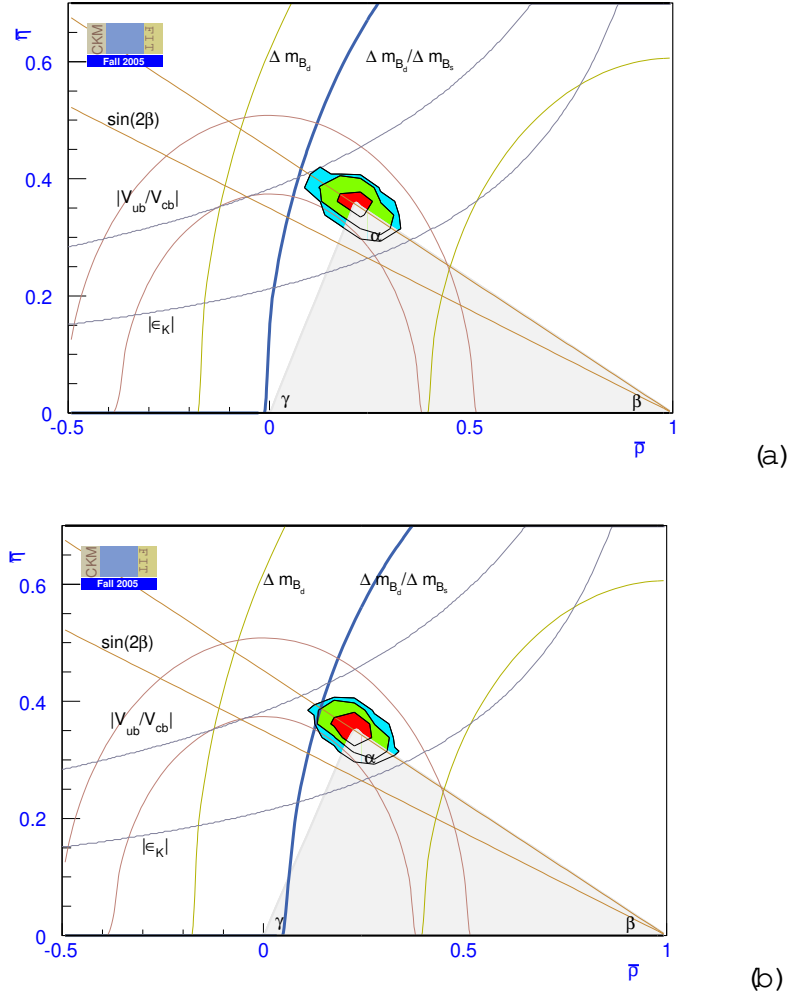


Figure 3: The first (a) of these plots represents the (β, γ) plane with the pre-Run II results and the second one (b) with the post-Run II results.

Although $F = 1$ processes such as the penguin transitions occurring in the charm-less decays $B \rightarrow \pi \pi \pi \pi$, which determine β and the CP asymmetries in semi-leptonic B decays ($B \rightarrow l \bar{\nu} X$) are important we do not consider these constraints here. The experimental constraint on β through the mentioned decays is currently sufficient even without necessarily assuming the SM but the relation $\beta = \gamma - \alpha$ is still used for this bound where α here comes from the decay amplitudes and γ from the $B_d \rightarrow B_d$ mixings, so this $F = 2$ process imposes already a good constraint on β . The CP asymmetry in semi-leptonic decays, A_{SL} is a crucial constraint of the UT analysis

because once r_{B_d} and m_{B_d} are defined through Eq. (12), the generalization of A_{SL} to account for BSM processes depends on r_{B_d} and m_{B_d} [37] at the NLO in the penguin term in the $F = 1$ amplitude. However the present experimental bounds are not precise enough to put constraints on r_{B_d} and m_{B_d} [11].

The two main fits that we have performed are the ones including the constraints $|V_{ub}|, |V_{cb}|, m_{B_d}, m_{B_s}, \sin 2\alpha$ and $\sin 2\beta$. The first one (a) using the available information from the $B_d^0 - B_s^0$ oscillation experiments for the summer conferences and the second one (b) using the data after the summer and fall conferences. As we have been pointing out, the increase on the lower bound on m_{B_s} due to averaging the fall data of the CDF and D0 collaborations with the rest of the collaborations (ALEPH, DELPHI and OPAL) by the Heavy Flavor Averaging Group (HFAG), has been shifted from $m_{B_s} > 14.5 \text{ ps}^{-1}$ to $m_{B_s} > 16.6 \text{ ps}^{-1}$. In Figure (3) (a) we present the 68%, 95% and 99% C.L. of the two dimensional pdf for α and β with the values of Tables (2) and (3) using the $m_{B_s} > 14.5 \text{ ps}^{-1}$ limit and in Figure (3) (b) using the $m_{B_s} > 16.6 \text{ ps}^{-1}$ limit.

As we can see in the (α, β) plane, the radius of the circle describing the constraint $m_{B_d} = m_{B_s}$ has been reduced and with it the overlap region of all the constraints, specially for $|V_{ub}|, |V_{cb}|$ and $\sin 2\alpha$. As a consequence the central value of α has been increased and the central value of β has been slightly reduced. In Figure (4) and Figure (5) we present the pdfs of α and β for these cases. As we can see by comparing these figures, the one dimensional (1d) pdf of α has been shifted to the right while the pdf of β has been left practically unchanged. In Figure (2) we present the m_{B_s} 1d projection using the (a) pre-Run II, (b) the t using post-Run II data and (c) it shown the output of m_{B_s} without using this constraint in the t .

Since now the limit on m_{B_s} it is closer to the region of maximal likelihood of the other constraints, although the change in α and β is not drastic, some of the parameters present an interesting change.

We compare how well the parameters defining a unitary triangle, R_b, R_t, α and β are fitted in each of the cases (a) and (b), by defining the quantities

$$R_t^2 = \hat{R}_t^2 - R_t^2; \quad R_b^2 = \hat{R}_b^2 - R_b^2 \quad (20)$$

analogously for the angles α and β , where \hat{R}_t and \hat{R}_b are computed as given in Eq. (2) with the values of R_t and R_b given by the t , as shown in Figures (4, 5), and R_t and R_b are the values as shown in Figures (6) and (6). We find that the t including the post-Run II (b) is fitted slightly better to the constraints on unitarity than the pre-Run II (a) t :

$$\begin{aligned} R_{ta}^2 &= 8.8 \cdot 10^{-4}; & R_{ba}^2 &= 2.4 \cdot 10^{-3}; \\ R_{tb}^2 &= 5.8 \cdot 10^{-4}; & R_{bb}^2 &= 1.7 \cdot 10^{-3} \\ \sin_a &= 1 \cdot 10^{-3}; & \sin_b &= 2.9 \cdot 10^{-3} \\ \sin_a &= 6.24 \cdot 10^{-3}; & \sin_b &= 3.37 \cdot 10^{-3}; \end{aligned} \quad (21)$$

Since α is determined through the constraint $\alpha = \alpha_{\text{unitary}}$, the difference \sin_a has no meaning for this kind of comparison.

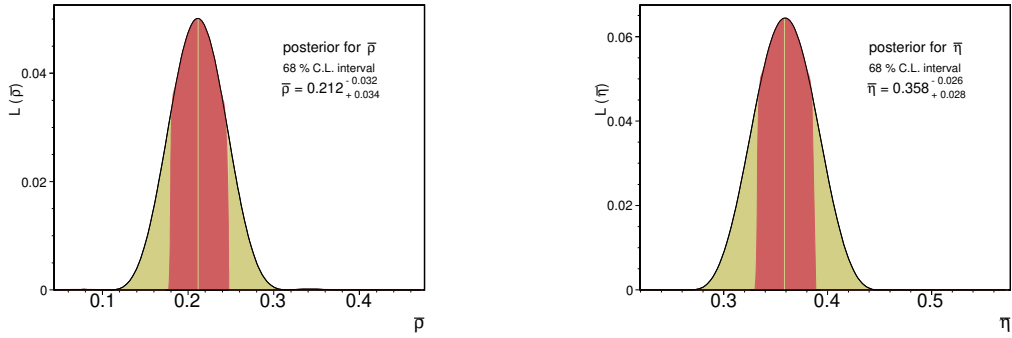


Figure 4: and one dimensional projections using the pre-R un II results.

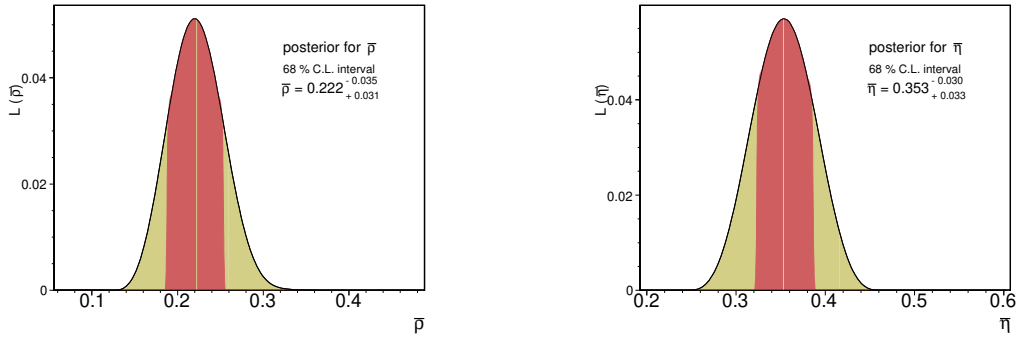


Figure 5: and one dimensional projections using the post-R un II results.

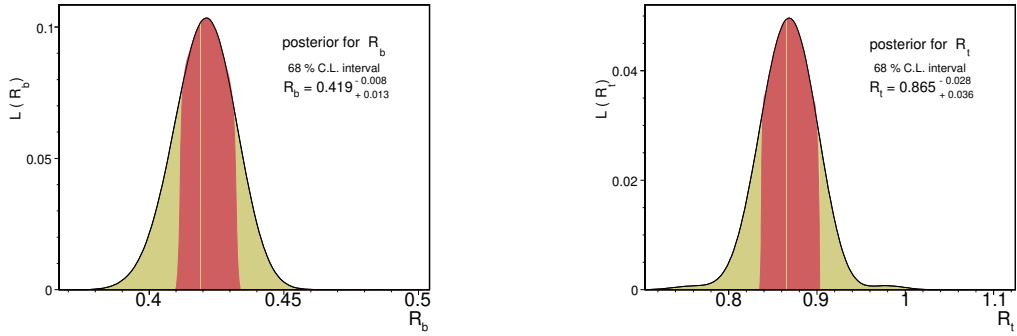


Figure 6: R_b and R_t one dimensional projections using the pre-R un II results.

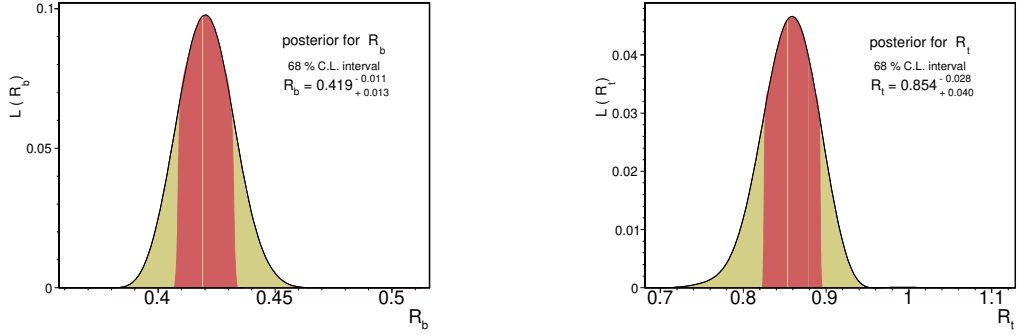


Figure 7: R_b and R_t one dimensional projections using the post-R un II results.

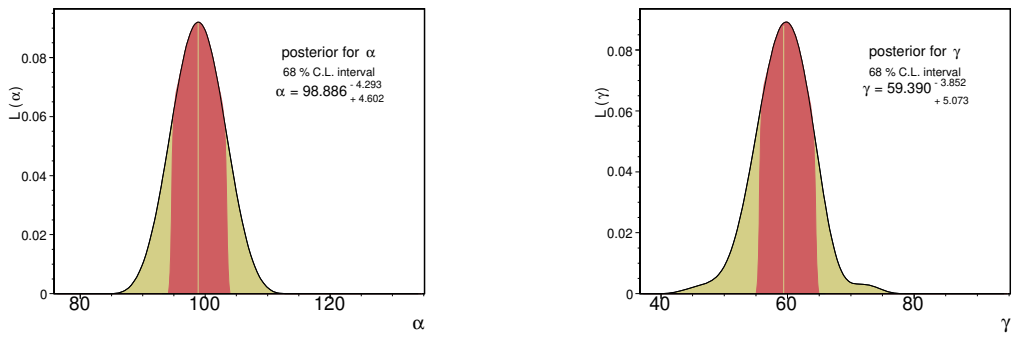


Figure 8: and one dimensional projections using the pre-Run II results.

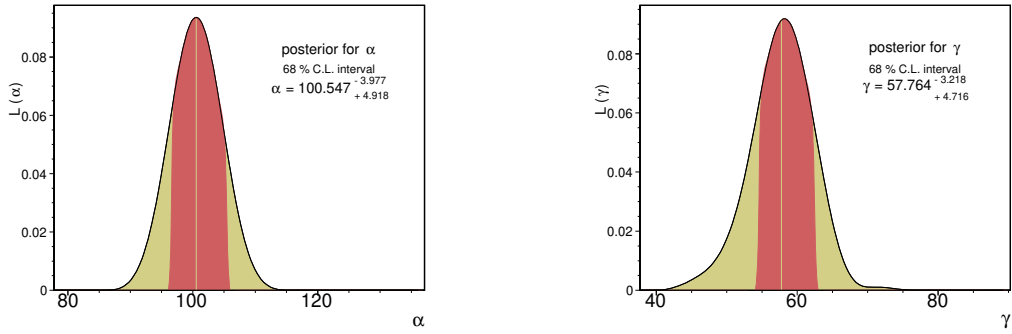


Figure 9: and one dimensional projections using the post-Run II results.

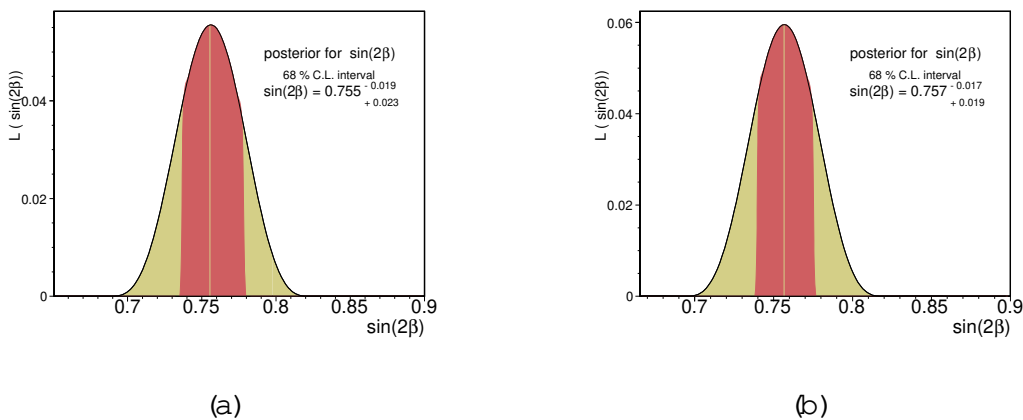


Figure 10: $\sin 2$ one dimensional projections using the (a) pre-Run II and (b) the t using post-Run II data.

6.2 Indirect evidence of CP violation

The analysis of the unitary triangle (UT) allows for the comparison of the t using only the CP conserving processes $\bar{V}_{ub} \bar{V}_{cb}$, m_{B_d} and $m_{B_d} = m_{B_s}$, with the current experimental values of the CP violation parameters κ and $\sin 2\beta$. This is a way to check how consistent is the t of the parameters that are sensitive just to the sides of the UT with respect to the measurements that are sensitive to the angles, which is an indirect measurement of the amount of CP violation. The (\bar{p}, \bar{p}) plane of this t is shown in Figure (6.2). We also compare the fitted 1d pdf's of the parameters κ and

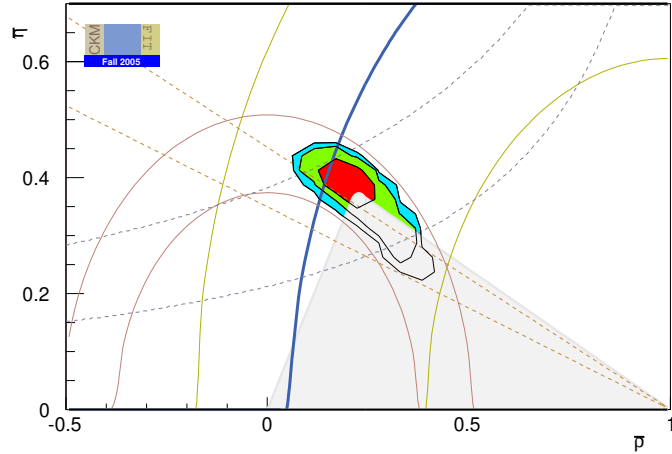


Figure 11: (\bar{p}, \bar{p}) plane with the post-RUN II results using only the CP conserving constraints $\bar{V}_{ub} \bar{V}_{cb}$, m_{B_d} and $m_{B_d} = m_{B_s}$. In dotted lines we have plotted the CP violating constraints: $\sin 2\beta$ and κ to compare them with the pdf of this t .

$\sin 2\beta$ to those given for the case when these parameters have been included in the t as a constraint. The output value of κ for the t including just $\bar{V}_{ub} \bar{V}_{cb}$, m_{B_d} and $m_{B_d} = m_{B_s}$ is $\kappa = (2.13; 3.017) \times 10^{-3}$ at 68% CL. It is perfectly consistent with its experimental value of $\kappa = (2.11; 2.45) \times 10^{-3}$ at 68% CL. However as we can see by comparing Figure (12 a) to Figure (10), both for the pre-RUN II and post-RUN II cases, the value of $\sin 2\beta$ increases if the CP violating constraints $\sin 2\beta$ and κ are not taken into account:

$$\sin 2\beta^{\text{CP conserv:}} = (0.772; 0.817); \quad (22)$$

leaving out the 68 % CL of the experimental measured value:

$$\sin 2\beta^{\text{exp}} = (0.655; 0.719); \quad (23)$$

This inconsistency is already apparent in the t s which include $\sin 2\beta$ and κ as a constraint, but here we note that the values of Eqs.(22) and (23) are consistent just at 95 % CL. One reason we observe this apparent inconsistency may be due to the current

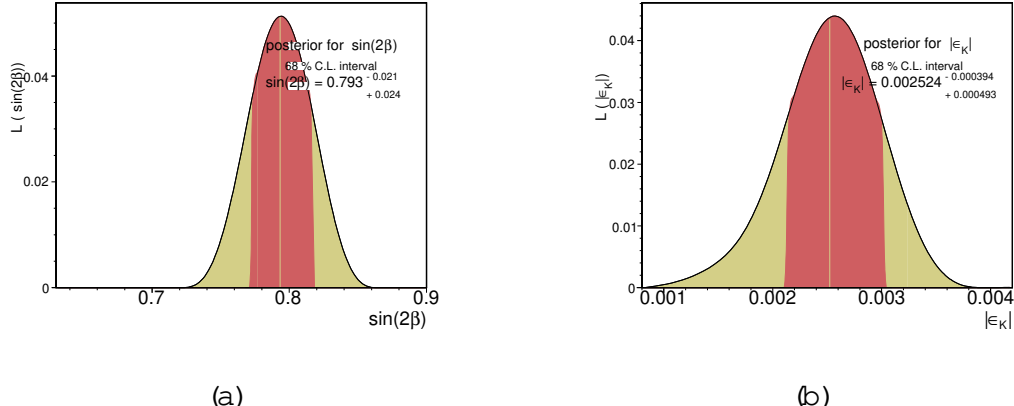


Figure 12: One dimensional projections of (a) $\sin 2\beta$ and (b) $|\epsilon_K|$ using post-Run II data without imposing them as a constraint.

set of experimental inputs for the constraints and their errors, especially for $|V_{ub}|=V_{cb}$. A better determination of these semi-leptonic parameters, it is crucial for checking this inconsistency. Another reason is that there is a non-zero phase accounting for processes BSM in $\sin 2\beta$ such that we have $\sin 2\beta = \sin(2\beta_{SM} + 2\beta_{B_d})$, as we have discussed in Section (3) and as we will be presenting in Section (7.3).

6.3 Determination of $f_{B_d}^2 \hat{B}_{B_d}$ and B_K

The actual measurement of m_{B_s} also provides a strong constraint on the non-perturbative QCD parameter $f_{B_s}^2 \hat{B}_{B_s}$ and through the relation Eq. (8) on the parameter $f_{B_d}^2 \hat{B}_{B_d}$, which suffers from big uncertainties. In particular here we can check how well the lattice computations of it,

$$f_{B_d}^2 \hat{B}_{B_d}^{QCD} = (0.223 \quad 0.033 \quad 0.012) \text{ GeV}; \quad (24)$$

agree with the present limit on m_{B_s} .

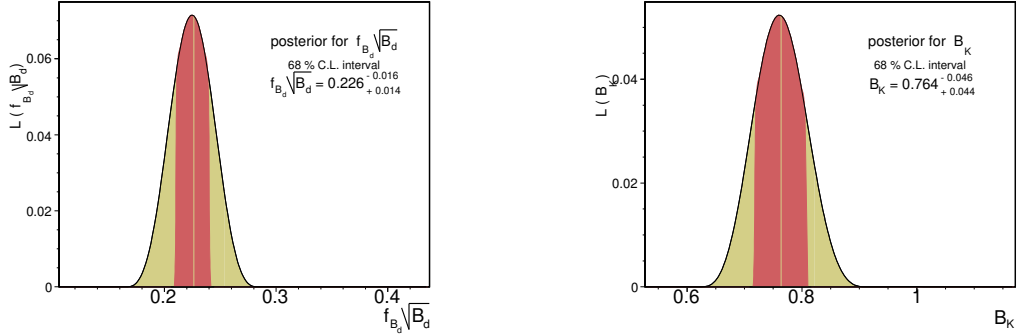


Figure 13: The pdf's for $f_{B_d}^2 \hat{B}_{B_d}$ and B_K for the pre-Run II fit.

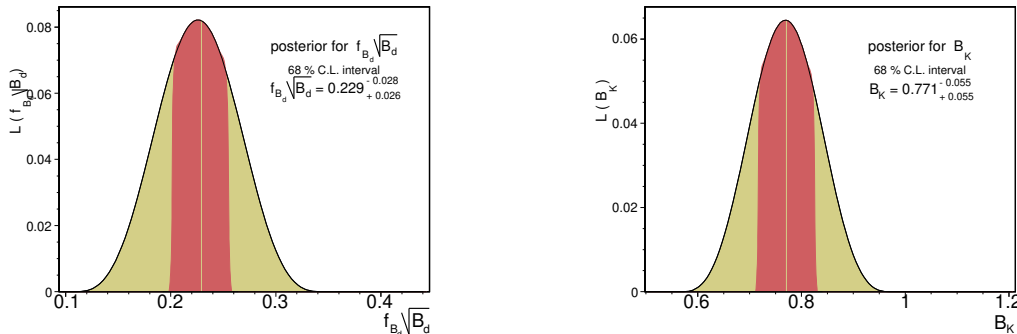


Figure 14: The pdf's for $f_{B_d}^2 \hat{B}_{B_d}$ and B_K for the post-Run II fit.

We can read the values of $f_{B_d}^2 \hat{B}_{B_d}$ from Figures (13) and (14). The value of these parameter for the overall fit are

$$f_{B_d}^2 \hat{B}_{B_d}^{\text{pre RunII}} = 0.226 \quad 0.016 + 0.014; \quad f_{B_d}^2 \hat{B}_{B_d}^{\text{post RunII}} = 0.229 \quad 0.028 + 0.026; \quad (25)$$

hence checking that the QCD Lattice value, Eq. (24), and the fit value of $f_{B_d}^2 \hat{B}_{B_d}$ agree remarkably well.

Comparing Figures (13) and (14) we can see that the post-Run II B_s^0 oscillation data has have an important impact on $f_{B_d}^2 \hat{B}_{B_d}$, by increasing its value and its

uncertainty, although this uncertainty is still determined to a better accuracy than the QCD determination, Eq. (24). The impact of m_{B_s} on B_K is not as strong as the impact on $f_{B_d}^2 \hat{B}_{B_d}$ since it is just affected through the overall t and not through a constraint, B_K only appears in the SM due to the j_K constraint, Eq. (9). Although the difference, B_K , between B_K as obtained in the t, Figures (13) and (14), and B_K as given by the QCD lattice calculations is smaller in the (b) post-Run II case,

$$\begin{aligned} B_K^{\text{QCD}} &= 0.79 \pm 0.04; \\ B_{K\text{ a}} &= 2.6 \pm 10^{-2} \\ B_{K\text{ b}} &= 1.9 \pm 10^{-2}; \end{aligned} \quad (26)$$

the uncertainty for the post-Run II case has been increased. It is interesting to compare the effect on B_K when j_K is removed as a constraint, as we can see in Figure (15), the value of B_K in this case is

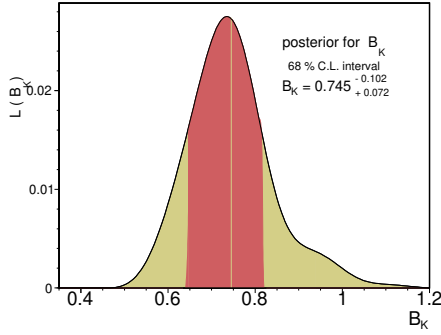


Figure 15: The pdf of B_K when j_K is not imposed as a constraint.

$$B_K = 0.745 \pm 0.102 \pm 0.072; \quad (27)$$

which agrees quite well with its QCD value, Eq. (26), although the error is of 12% in contrast with the 10% error of the QCD calculation.

7 Bounds on processes B SM

7.1 Scenario I

In this scenario we consider the constraints on models for which the conditions of what has been called Minimal Flavour Violation (MFV) are valid. A effective theory is said to be minimal flavour violating if all higher-dimensional operators constructed from the SM and fields responsible for giving the corresponding structure of Yukawa couplings (e.g. avon-scalar-fields which vevs determine the effective Yukawa couplings) are invariant under the CP symmetry and the flavour symmetry, determined by the group G_F . When this happens then the dynamics of flavour violation is completely

determined by the structure of the SM Yukawa couplings. If all Yukawa couplings are small except for the top, then the only relevant non-diagonal operators entering in the Hamiltonians of the $F = 2$ transitions are proportional to $Y_u Y_u^Y \sum_{ij} Y_t^2 V_{ti} V_{tj}$. By looking at Eq. (14) we can see that $V_{td} V_{tb}$ and $V_{td} V_{ts}$, the main contribution to the mixings in the $B = 2$ and $S = 2$ transitions respectively, are multiplied by the same Inami-Lim function $S(x_t)$ (as expressed in Eq. (5) and Eq. (9)) exactly because of the top dominance. Once there is another particle contributing at the same order of the top contributions then the expressions of the dominating diagrams for the processes $B = 2$ and $S = 2$ become different. This is evident in supersymmetric theories when $\tan \theta_s$ is large because the bottom contribution becomes relevant and hence it gives a sizable contribution to the $B = 2$ transitions. Due to the potential difference in these processes, two possibilities are considered:

- (i) $S(x_t) \neq S(x_t) + S(x_t)$
- (ii) ${}_2 S(x_t) \neq {}_2 [S(x_t) + S(x_t)]$,
 ${}_B S(x_t) \neq {}_B [S(x_t) + S(x_t)]$

7.1.1 Example: supersymmetric MFV scenario in the low $\tan \theta_s$ limit

In the context of MSSM models there are four physical phases: ϕ_{km} , $\alpha_A = \arg(A)$, $\beta = \arg(\beta)$ and the QCD vacuum parameter ϕ_{QCD} which however can be conveniently set to be zero.

Experimental upper limits on the electric dipole moments (EDM) of the neutron and electron provide constraints on the phases ϕ_{km} and α_A . In the constrained minimal supersymmetric standard model (CMSSM) in general the bounds on ϕ_{km} are stronger than those to α_A , where ϕ_{km} ranges from $0(10^{-1})$ to $0(10^{-4})$ [17]. In the minimal SUGRA model $\phi_{km} \approx 0(10^3)$ while α_A can be $0(1)$ in the small $\tan \theta_s$ region [19].

At which extend ϕ_{B_d} and ϕ_s are affected by these bounds depend on the values of $\tan \theta_s = v_u/v_d$, the ratio of the vacuum expectation values of the two Higgs fields in the MSSM. For low-to-moderate values of $\tan \theta_s$ in SUGRA models α_A does not show up in the phase of either the matrix elements $hB_d^0 \rightarrow H_{eff}^{SUGRA} B_d^0 i$ and $hK_0 \rightarrow H_{eff}^{SUGRA} K_0 i$, hence

$$\begin{aligned} \arg hB_d^0 \rightarrow H_{eff}^{SUGRA} B_d^0 i &= \arg (V_{td} V_{tb}); \\ \arg hK_0 \rightarrow H_{eff}^{SUGRA} K_0 i &= \arg (V_{td} V_{ts}); \end{aligned} \quad (28)$$

thus ϕ_{B_d} , ϕ_s and ϕ_{km} can be safely treated as zero in this case. This means that CP violation asymmetries give information just for β and ϕ_s as defined in the SM and the BSM contribution to α_A is aligned with the tt contribution of the SM $\arg(V_{td} V_{ts})$. In this context then the analysis of the UT and CP violation phases β and ϕ_s can be carried out in a very similar way as in the SM, just by taking into account the contributions to $(V_{td} V_{tb})$ and $(V_{td} V_{ts})$ without involving additional phases to those in the MSSM models. For large $\tan \theta_s$ cases it is necessary to take into account new operators whose

contributions become relevant for this case. These contributions can be computed for a given theory from the effective Hamiltonian $H_{\text{eff}}^{(B=2)} = \frac{G_F^2 M_W^2}{2^2} \sum_{i=1}^3 C_i(\lambda) Q_i$, where C_i are the Wilson coefficients and the operators Q_i are given by

$$Q_1 = d_L b_L d_L \bar{d}_L; \quad Q_2 = d_L b_R d_L \bar{b}_R; \quad Q_3 = d_L b_R d_R \bar{b}_R; \quad (29)$$

The first two operators are as in the SM, while the supersymmetric contributions to Q_3 from which chargino contributions to $C_3(\lambda)$ are generically complex relative to the SM contribution and hence can generate a new phase shift in the $B^0 \rightarrow B^0$ mixing amplitude. This is quite significant because $C_3(\lambda) / \frac{m_b}{m_W} \cos^2 \theta_W$. When the EDM constraint in these cases is imposed m_{B_d} becomes very small [23], [24].

If we would like to accurately test the possible theory for physics beyond the SM, we have to compute all the quantities involved in the box diagrams associated to these mixings. Precisely the NLO QCD parameters in the supersymmetric MFV context required for m_{B_d} , m_{B_s} and m_K have been calculated under the following simplifications [28]: (i) The s-quark flavour mixing matrix which diagonalizes the s-quark mass matrix is approximately the same as the V_{CKM} , apart from the left-right mixing of the top quarks. (ii) The first and second generations s-quarks with the same gauge quantum numbers remain highly degenerate in masses but the third generation (especially t) can be significantly lighter due to RGE of the top Yukawa couplings. (iii) The phases of d_s can be safely set to zero in the entire $\tan \beta$ space once the EDM constraint is imposed (considered first in [22]). Then m_{B_d} can be expressed as

$$m_{B_d} = \frac{G_F^2 M_W^2}{2^2} m_{B_d} f_{B_d}^2 \hat{B}_{B_d} [A_{SM}(B) + A_H(B) + A_s(B) + A_g(B)]; \quad (30)$$

where $A_{SM}(B) = S(x_t) j_{tq} j_{tb} \frac{\partial}{\partial B}$.

The expressions for $A_H(B)$, $A_s(B)$ and $A_g(B)$ are obtained from the SUSY box diagrams. Here, H , j , t_a and d_i represent, respectively, the charged Higgs, chargino, s-top and s-down-type s-quarks. The contribution of the intermediate states involving neutralinos is small and usually neglected. The expressions for $A_H(B)$, $A_s(B)$ and $A_g(B)$ are given explicitly in [25], [18], [12].

Similarly in this context j_K can be expressed by:

$$j_K = C B_K [\text{Im } A_{SM}(K) + \text{Im } A_H(K) + \text{Im } A_s(K) + \text{Im } A_g(K)]; \quad (31)$$

where, the constant C and $\text{Im } A_{SM}$ are as given in Eq. (9) and the expressions for $\text{Im } A_H(K)$, $\text{Im } A_s(K)$ and $\text{Im } A_g(K)$ can be found in [25], [18], [12].

In the MFV context, [26], apart from the SM degrees of freedom, only charged Higgs fields, charginos and a light s-top (assumed to be right-handed) contribute, with all other supersymmetric particles integrated out. This scenario is effectively implemented in a class of SUGRA models (both minimal and non-minimal) and gauge-mediated models [27] in which the first two s-quark generations are heavy and the contribution from the intermediate gluino-s-quark states is small [19, 20, 16, 21, 18].

The phenomenological profiles of the unitary triangle and CP phases for the SM and this class of supersymmetric models can thus be meaningfully compared. Given the high precision on the phases, and expected from experiments at B-factories and hadron colliders, a quantitative comparison of this kind could provide means of discriminating between the SM and this class of MSSM's.

In the next subsections we follow the work of Krauss and So [28] in order to identify the NLO QCD supersymmetric contributions to the $F = 2$ processes.

7.1.2 NLO QCD-corrected effective Hamiltonian for $B = 2$

The NLO QCD-corrected effective Hamiltonian for $B = 2$ transitions in the minimal flavour violation SUSY framework can be expressed as follows at the bosonic scale $= O(m_{B_d}^2)$ [28]:

$$H_{\text{eff}}^{(B=2)} = \frac{G_F^2}{4^2} (V_{td} V_{tb})^2 \gamma_2(B) () S Q_1() ; \quad (32)$$

where Q_1 is given in Eq. (29), S is a sum of the Landau-Lipman functions for the different internal particles, $S = S(x_W; x_H) + S(x_i; y_a)$ ⁴, where

$$x_{W,H} = \frac{m_t^2}{M_W^2; H} ; x_{d,s,c,b} = \frac{m_{d,s,c,b}^2}{M_W^2} ; y_a = \frac{m_{q_a}^2}{M_W^2} ; x_i = \frac{m_{\tilde{x}_i}^2}{M_W^2} \quad (33)$$

$Q_1()$ and $\gamma_2(B;)$ depend on the scale but once they are run down to the electroweak scale $= M_W^2$ and the matching conditions are performed, then the NLO QCD correction factor $\gamma_2(B)$ can be expressed as [28]:

$$\gamma_2(B) = \gamma_s(m_W) \overset{(0)}{=} (2 \overset{(0)}{n_f}) \frac{\#}{1 + \frac{s(m_W)}{4} \frac{D}{S} + Z_{n_f}} ; \quad (34)$$

in which n_f is the number of active quark flavours (here $n_f = 5$), $Z_{n_f} = \frac{\overset{(1)}{n_f}}{2 \overset{(0)}{n_f}} - \frac{\overset{(0)}{n_f}^2}{2 \overset{(0)}{n_f}^2} \overset{(1)}{n_f}$, and $\overset{(0)}{n_f}$ and $\overset{(0)}{n_f}$ are the anomalous dimension and beta functions of QCD⁵ with $N_c = 3$ and $C_F = 4/3$. The function D comes from identifying the QCD correction factor once the Wilson Coefficient is computed (in the naive dimensional regularization scheme using \overline{MS}) and is a function of Eq. (33), $D = D(x_W; x_H; x_0) + D'(f x_i; y_a; x_0)$. The factor $[1 + \frac{s(m_W)}{4} \frac{D}{S} + Z_{n_f}]$ is quite stable against variations of the functions D and S and has been found to be [28] and [22], around 0.89 and hence $\gamma_2(B)$ is found to be $\gamma_2(B) = 0.51$ in the \overline{MS} scheme.

⁴ $S(x_W; x_H) = S_{W,W}(x_W) + 2S_{W,H}(x_W; x_H) + S_{H,H}(x_H)$ and
 $S'(f x_i; y_a g) = \sum_{i,j=1, a,b=1}^5 K_{ij,ab} S(x_i; x_j; y_a; y_b)$
 $\overset{5}{h}^{(0)} = \frac{6N_c - 1}{N_c} ; \overset{(0)}{n_f} = \frac{11N_c - 2n_f}{3} , \overset{(1)}{n_f} = \frac{34}{3} N_c^2 - \frac{10}{3} N_c n_f - 2C_F n_f , \overset{(1)}{n_f} = \frac{N_c - 1}{2N_c} 21 + \frac{57}{N_c} \frac{19}{3} N_c + \frac{4}{3} n_f .$

The Hamiltonian given above for $B_d^0 \{ \overline{B_d^0} \}$ mixing leads to the mass difference

$$m_{B_d} = \frac{G_F^2}{6^2} (V_{td} V_{tb})^2 \gamma_2(B) S f_{B_d}^2 B_{B_d}; \quad (35)$$

analogously for m_{B_s} . Since in the MFV supersymmetric context, the QCD correction factors are identical for m_{B_d} and m_{B_s} then m_{B_d} and m_{B_s} have the same enhancement, with respect to their values in the SM. Hence the ratio m_{B_s}/m_{B_d} is the same as in the SM.

7.1.3 NLO QCD-corrected effective Hamiltonian for $S = 2$

The NLO QCD-corrected Hamiltonian for $S = 2$ transitions in the MFV framework has also been obtained in Ref. [28]. From this, the result for $j_K j$ can be written as:

$$j_K j = C_{B_K} A^{2/6} [\gamma_1(x_c) + A^{2/4} (\gamma_2(K) S + \gamma_3 S(x_c; x_t));$$

where the NLO QCD correction factor is [28]:

$$\gamma_2(K) = \frac{\gamma_1(m_c)^{(0)} = (2/3)}{1 + \frac{\gamma_1(m_c)}{4} (Z_3 - Z_4)} + \frac{\gamma_1(m_b)^{(0)} = (2/4)}{1 + \frac{\gamma_1(m_b)}{4} (Z_4 - Z_5)} + \frac{\gamma_1(M_W)^{(0)} = (2/5)}{1 + \frac{\gamma_1(M_W)}{4} (\frac{D}{S} + Z_5)}; \quad (36)$$

again as it happens with $\gamma_2(K)$, the factor involving the functions Z_i, D and S , is quite stable and has been calculated, [28] [22], to give 0.84, consequently $\gamma_2(K)$ is estimated to give $\gamma_2(K) = 0.53$ in the \overline{MS} scheme.

7.1.4 Effects of MFV for m_{B_d} and K

Here we summarize the effects of MFV for the transitions $B = 2$ and $S = 2$ with respect to the SM it is characterized by the shifts

$$\begin{aligned} \gamma_B S(x_t) &= \gamma_2(B) S; \\ \gamma_S S(x_t) &= \gamma_2(K) S; \end{aligned} \quad (37)$$

where $\gamma_2(B)$, $\gamma_2(K)$ and S are functions of $(m_{\tau_2}; m_{\tau_2}; m_H; \tan \beta)$. In Section (7.3.2) we are going to use the approximations of [22] and [28] for $\gamma_2(B)$ and $\gamma_2(K)$

$$\begin{aligned} \gamma_2(B) &= 0.51; \\ \gamma_2(K) &= 0.53 \end{aligned} \quad (38)$$

and compute explicitly S for different supersymmetric inputs.

7.2 Scenario II

In this context we can test models for which the SM contribution to K is considerably larger than the corresponding contribution to m_{B_d} and m_{B_s} or vice-versa. Hence we can expect variations of the top-W box diagram function, $S(x_t)$, different for m_{B_d} (or m_{B_s}) and for K .

An example of this possibility occurs in models with a horizontal symmetry where often the CKM matrix is no longer the only source of CP violation because there are off-diagonal elements in the soft squared matrices as well as in the trilinear terms. In this respect these models depart from the condition of MFV since the dynamics of flavour violation is no longer completely determined from the structure of the SM Yukawa couplings. However if the models behave in the low energy limit as a supersymmetric extension of the SM, i.e. all other fields not being the SM fields and their supersymmetric partners have been integrated out at the scales where the supersymmetry is broken; then we can describe m_{B_d} and K as in Eq. (30) and Eq. (31) respectively where we can have sizable contributions for example from the gauginos.

In [42] we have constructed and analyzed the predictions of a supersymmetric model with an underlying SU(3) horizontal symmetry and with spontaneous CP violation. A full numerical analysis of this type of models, including the exact diagonalization of the soft mass matrices, is still due to but since in the context of the Mass Insertion approximations (MI)⁶ the $F = 2$ Hamiltonian can be expressed [39] in terms of $\frac{d}{LL}$, $\frac{d}{RR}$, $\frac{d}{LR}$ and $\frac{d}{RL}$, we have compared the experimental bounds with the predictions of the model. The model puts the following limits

$$q \frac{\frac{q}{\text{Im}(\frac{d}{RR})_{12}}}{\frac{q}{[\text{Im}(\frac{d}{RR})_{12}(\frac{d}{LL})_{12}]}} \quad 6.8 \quad 10^{-4} \sin \theta_1 \\ 2 \quad 10^{-4} \sin \theta_1; \quad (39)$$

where θ_1 is a phase of the model, preferably small. These limits can be compared with the experimental limits, obtained in the Kaon sector, of $\text{Im}(\frac{d}{RR})_{12} \approx 3.2 \cdot 10^{-3}$ and $[\text{Im}(\frac{d}{RR})_{12}(\frac{d}{LL})_{12}] \approx 2.2 \cdot 10^{-4}$, which correspond to average s-quark masses of $m_q = 500$ GeV and they can scale as m_q GeV = 500, so we can see that they large values of m_q , they can give a large contribution to K , but as we will see for the current results on possible contributions of non SM physics to K , these are rather small, limiting the possibilities of a big contribution to K from these kind of theories. In the B sector the contributions can be negligible, so this is an example in which K can receive big contributions, while m_{B_d} is left practically unchanged.

⁶Defined by $\frac{q}{A_B} = \frac{V_A^{qY} M^{-2} V_B^q}{m_q}$, where A;B = L;R refers to the chirality of the superpartners of the internal lines of the relevant F processes and V_A^q are the matrices diagonalizing the Yukawa couplings, e.g. $Y_{\text{diag}}^d = V_L^{dy} Y^d V_R^d$

7.3 Results

7.3.1 Procedure to extract information on bounds B SM

The procedure to obtain the pdf's for r_{B_d} , r_{B_d} and r_K it is the very simple observation than we can write these parameters as

$$\begin{aligned} r_{B_d} &= \frac{m_{B_d}^{\exp}}{q_{m_{B_d}} S(x_t)}; \quad \sin(2^{SM} + 2_{B_d}) = \sin 2^{\exp}; \\ r_K &= \frac{K^{\exp}}{q_{K,1} + q_{K,2} S(x_t)}; \end{aligned} \quad (40)$$

where $q_{m_{B_d}}$, $q_{K,1}$ and $q_{K,2}$ are functions of the Wolfenstein parameters (and of the correspondent transitions $B = 2$ and $S = 2$) so we can extract the pdf for r_{B_d} and r_K as $p(r) / p(r)$, exactly as in the case of the parameters of the Classic Fit, Eq. (17). The most conservative way to obtain r_{B_d} , r_{B_d} and r_K is to use only the constraint $\mathcal{V}_{ub} \neq \mathcal{V}_{cb}$ and experimental constraints on r_K and r_{B_d} , such as the decays $B \rightarrow D \bar{K}$ and $B \rightarrow D \bar{K}$ for $F = 1$ processes. However we use the constraint $m_{B_s} = m_{B_d}$ for two reasons: the first one is to study the impact on the new bound on m_{B_s} and to probe the models for which this ratio is left invariant, such as the MFV case. In order to present the impact on the parameters measuring processes B SM we perform the following series of tests.

- (i) Constraints $\mathcal{V}_{ub} \neq \mathcal{V}_{cb}$, $\sin 2^{\exp}$, $m_{B_s} = m_{B_d}$ and m_{B_d} to obtain r_K ,
- (ii) Constraints $\mathcal{V}_{ub} \neq \mathcal{V}_{cb}$, $m_{B_s} = m_{B_d}$ and r_K to obtain $r_{m_{B_d}}$ and r_{B_d} ,
- (iii) Constraints $\mathcal{V}_{ub} \neq \mathcal{V}_{cb}$, $\sin 2^{\exp}$, $m_{B_s} = m_{B_d}$ to obtain r_K , $r_{m_{B_d}}$ and r_{B_d} .

In the (iii)-th case, r_{B_d} should be consistent with zero at some CL since we are imposing the $\sin 2^{\exp}$ constraint. From these tests we can extract then information for bounds on the examples presented in the previous section.

7.3.2 Outputs

- (i) Results using the constraints $\mathcal{V}_{ub} \neq \mathcal{V}_{cb}$, $\sin 2^{\exp}$, $m_{B_s} = m_{B_d}$ and m_{B_d}

The results of this test are relevant to probe the models for which m_{B_d} is expected to be left invariant while a change in r_K may happen, as it is the case of the SU(3) flavour models [42], as pointed out in Section (7.2). First we can check that the experimental value of r_K lies within a third of the 68% CL of the output value of r_K : $2.454_{-0.367}^{+0.422} \cdot 10^{-3}$. Then we see that r_K is compatible with unity:

$$r_K = 0.951 \quad 0.150 \pm 0.117 \quad (41)$$

although the uncertainty in this parameter is about 14% of its value. Taking into account that the uncertainty in the hadronic parameter B_K is of about 12%, since

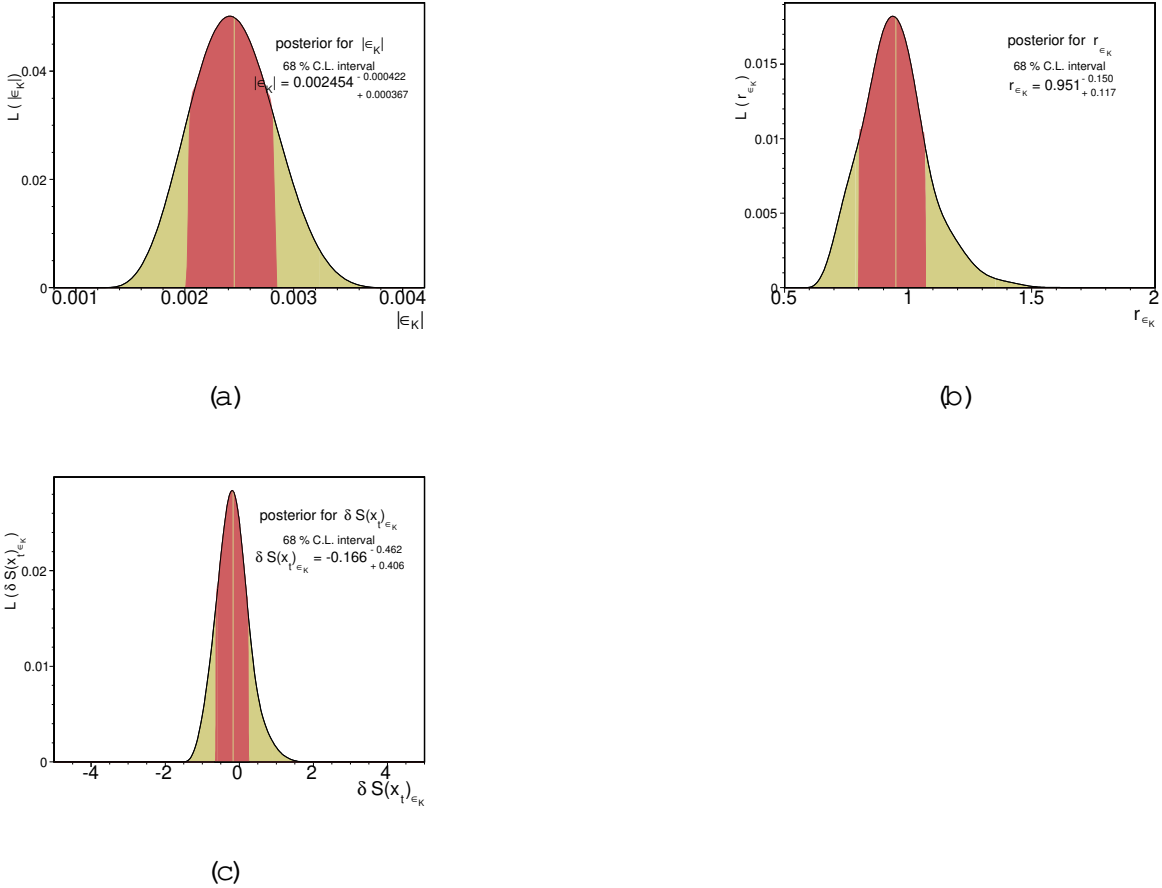


Figure 16: One dimensional probabilities for (a) $|\epsilon_K|$, (b) r_{ϵ_K} and (c) $S(x_t)_{\epsilon_K}$ when ϵ_K is not imposed as a constraint.

$B_K = 0.79 \pm 0.004 \pm 0.09$, we see then that the uncertainty in the determination of r_{ϵ_K} is due to the uncertainty on B_K , since indeed we can only determine it with a good accuracy $r_{\epsilon_K} B_K$. However it is important to remark that the value of r_{ϵ_K} does not cluster exactly around 1, which leaves interesting possibilities of processes BSM in this case. For the example of SU(3) model presented in Section (7.2) we see that if this model is to satisfy the present determination of r_{ϵ_K} then the s-quark masses should not exceed 500 GeV and the phase χ_1 should be quite small.

In the general context of MFV D'Ambrusio et. al. [13] have classified the operators for which we can expect contributions BSM. In particular for the $F = 2$ operators, O_n the effective Hamiltonian can be written as

$$H_{\text{eff}} = \frac{1}{2} \sum_n a_n O_n + h.c.; \quad \frac{p_F}{2} \frac{G_F}{\sin^2 \theta_W} \sum_n V_{ti} V_{tj} C_n Q_n + h.c.; \quad (42)$$

where p is the scale at which the operators become relevant and a its effective coefficient. The term after the arrow is the standard notation for the Hamiltonian using the

Wilson coefficients C_n and the QCD operators Q_n . The Hamiltonian in Eq. (42) can be normalized such that the electroweak contributions is of order one, i.e. for the SM $a_{SM} = 1$ and the scale $s_{SM} = \sqrt{s}$ can be defined such that $\sqrt{s} = y_t \sin^2 \theta_W M_W = 2.4$ TeV. Hence we consider the ratios r_{B_d} and r_K , defined through Eq. (12), we are getting a measure of $(\frac{r}{r_{SM}})^2$. In particular

$$S(x_t) = \frac{4a}{a_{SM}} \frac{r_{B_d}}{r_{SM}}^2; \quad (43)$$

such that we can put bounds on the scale at which a process B SM could take place, by considering $a = 1$. For this case, taking into account the full 68% C.L. range, the bounds for r_{B_d} are > 6.16 TeV for a negative $S(x_t)$ contribution with respect to the SM contribution and > 9.8 TeV for a positive contribution.

(ii) Results using the constraints $\mathcal{V}_{ub} \neq \mathcal{V}_{cb}$ and $m_{B_s} = m_{B_d}$ and r_K

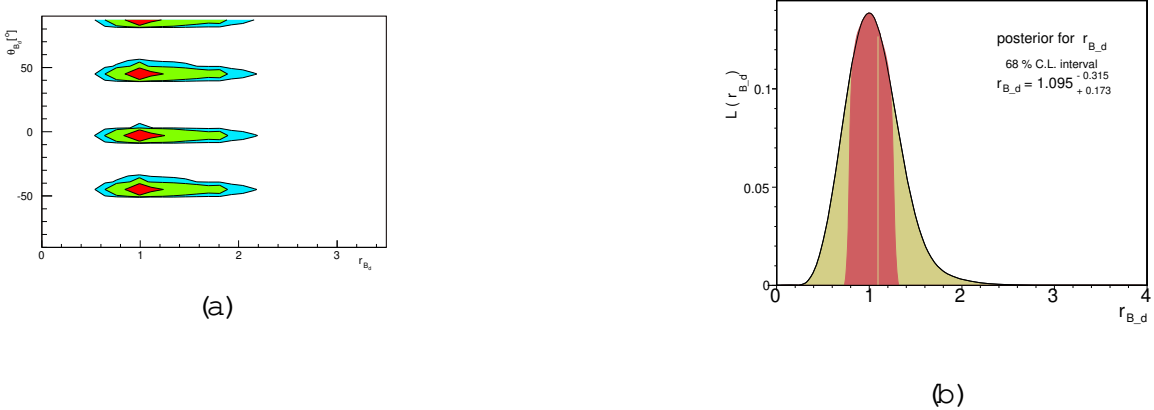


Figure 17: The two dimensional probability (a) for r_{B_d} and r_{B_d} and the one dimensional probability (b) for r_{B_d} . As we can see this solution agrees remarkably well with the SM, for which $r_{B_d} = 1$ and $r_{B_d} = 0$, although there could be a phase different from zero, giving new contributions to the phase and δ , see Figure (18).

Here it is important to compare the output value of the t for m_{B_d} to its experimental counter part and to the output of the complete t to check that this t is consistent with the experimental value. The output values of m_{B_d} for this t and the complete t are respectively

$$m_{B_d} = (0.497 \pm 0.047 \pm 0.017) \text{ ps}^{-1}; \quad m_{B_d} = (0.502 \pm 0.136 \pm 0.104) \text{ ps}^{-1};$$

which has to be compared to $m_{B_d} = (0.506 \pm 0.005) \text{ ps}^{-1}$, so we can see that the output value of m_{B_d} agrees remarkably well with its experimental counterpart, consequently the output value of r_{B_d}

$$r_{B_d} = 1.095 \pm 0.315 \pm 0.173; \quad (44)$$

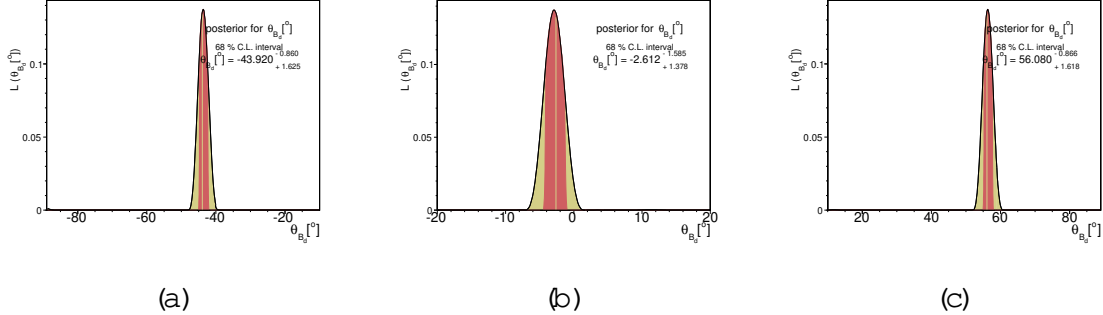


Figure 18: The possible solutions for the phase θ_{B_d} in the range $(-90; 90)^\circ$: (a) and (c) are non SM solutions while (b) it is compatible with the SM (ie $\theta_{B_d} = 0$) at 95% CL.

clusters around 1, although it has an uncertainty of about 23% its value, which leaves some possibilities for processes BSM. We can check this also by looking at the 1d projections of the possible phases for this case, in Figure (18) we show the possible solutions for the phase θ_{B_d} in the range $(-90; 90)^\circ$: (a) and (c) are non SM solutions. The solution (b), for which

$$\theta_{B_d} = (2.61 \pm 1.38)^\circ; \quad (45)$$

it is compatible with the SM, for $\theta_{B_d} = 0$ only at 95% CL. This points out to the interesting possibility of having a contribution to the angles and , through the relation Eq. (13), while no contribution BSM to m_{B_d} .

(iii) Results using the constraints $\bar{Y}_{ub} \neq \bar{Y}_{cb} \neq \sin 2\theta$ and $m_{B_s} = m_{B_d}$

The results of this t can be used to test the hypothesis of M FV violation and specifically the supersymmetric case, with the extra assumptions mentioned in Section (7.1). In these cases it is assumed that m_{B_d} and $j_K j_W$ will have the same change in $S(x_t)$, the box diagram function of the top-W boson interaction, thus in general we can compare r_K and r_{B_d} as defined in Eq. (1), whose values can be read from Figure (7.3.2) and Figure (7.3.2) respectively:

$$r_K = 1.211 \pm 0.195 \pm 0.280; \quad r_{B_d} = 1.258 \pm 0.422 \pm 0.354; \quad (46)$$

and hence extract $S(x_t)_K$ and $S(x_t)_{m_{B_d}}$ which are

$$S(x_t)_K = 0.684 \pm 0.565 \pm 0.932; \quad S(x_t)_{m_{B_d}} = 0.587 \pm 0.950 \pm 0.846; \quad (47)$$

that are in agreement with the hypothesis of M FV, although the uncertainties are big.

According to Eq. (43) the limits on r from Eq. (47) are for K : > 4.6 TeV. In the 68% CL range in this case $S(x_t)_K$ is a positive contribution. For m_{B_d} : > 8 TeV for a negative contribution with respect to the SM and > 4 TeV for a positive contribution.

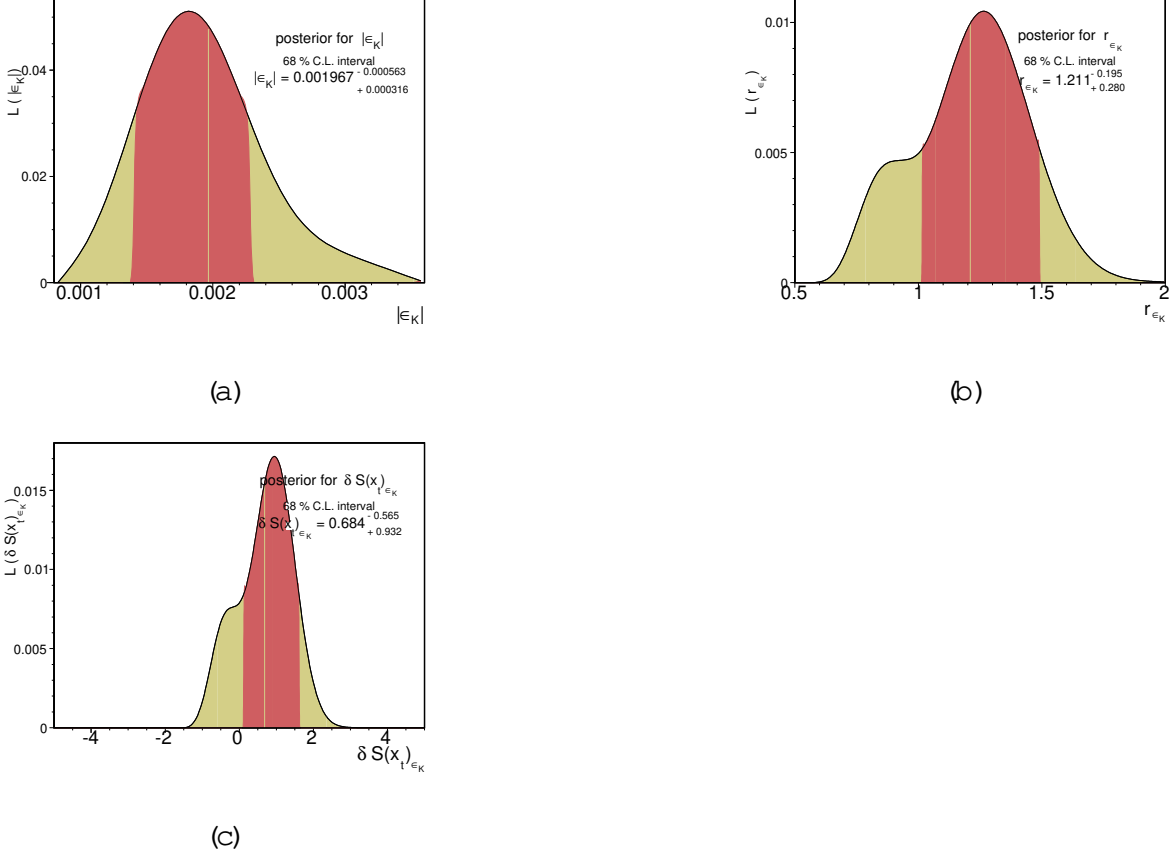


Figure 19: One dimensional probabilities for (a) $|\epsilon_K|$, (b) r_{ϵ_K} and (c) $\delta S(x_t)_{\epsilon_K}$ when K and m_{B_d} are not imposed as constraints for the t .

For the case of the supersymmetric MFV we can say more, since we have the change of Eq. (37), thus we can determine to which values of ${}^2(B)$, ${}^2(K)$ and S the parameters determined from the fits correspond to

$$\begin{aligned} S &= r_{B_d} \frac{B}{{}^2(B)} S(x_t) &= 3.0006_{-0.8444}^{+1.0065}; \\ S &= \frac{\tau t}{{}^2(K)} [S(x_t) + S(x_t)_K] = 3.2062_{-1.0800}^{+0.6819}; \end{aligned} \quad (48)$$

where we have used the following values for $S(x_t)$:

$$S(x_t) = 2.2764 \quad 0.06466 + 0.0652; \quad (49)$$

taking into account the uncertainty in the value of the top mass at M_W , $S(x_t)$. The values of τt and B can be read from Table (2). The values of ${}^2(B)$ and ${}^2(K)$ are given in Section (7.1.1) in Eq. (38).

We can determine values of S , with a given input of representative supersymmetric extra-constraints to the MFV hypothesis. In Table (1) we present some of these

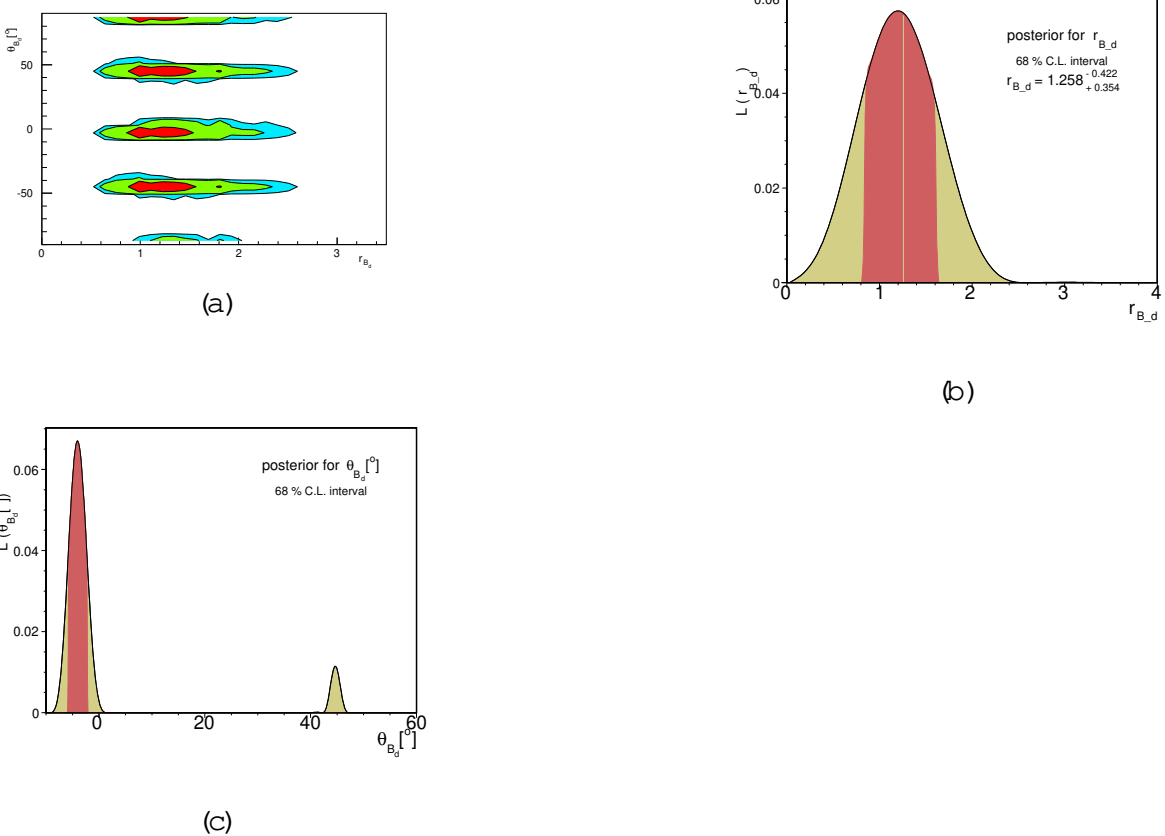


Figure 20: In figure (a) we have presented the contour levels of r_{B_d} versus θ_{B_d} at 99%, 95% and 68%. In (b) the one dimensional pdf of r_{B_d} and in (c) the one dimensional pdf of the solution for θ_{B_d} compatible with the SM, whose 68% CL is $(5.99; 2.17)^\circ$ with mean at 4.03° and another solution whose 68% CL is $(43.01; 46.21)^\circ$ at 44.64° .

examples, which need to satisfy the conditions

$$\begin{array}{ll}
 150 \text{ [GeV]} & m_{\tilde{t}_R} \quad 300 \text{ [GeV]}; \quad m_{\tilde{t}_L} \quad m_{\tilde{u}_L} \quad 600 \text{ [GeV]}; \\
 & m_{\tilde{t}_L} \quad m_{\tilde{q}} \quad 900 \text{ [GeV]}; \\
 100 \text{ [GeV]} & m_{\tilde{e}_2}; \quad m_{\tilde{e}_1} \quad 400 \text{ [GeV]}; \\
 \end{array} \quad (50)$$

for $m_{\tilde{q}} = m_{\tilde{e}_{1,2,4,5}}$. We can see that larger values of S correspond to small values of $\tan\beta$ and a heavy supersymmetric spectra, except for the charginos, which can be somewhat lighter than the rest of the involved sparticles. From the examples presented the ones for $\tan\beta = 5$ and the rest for $\tan\beta = 8$ are in agreement with the determination of S from the observed values of r_{B_d} , $S(x_t)$ and $S(x_{\tilde{t}})$ at 68% CL, while the last solution for $\tan\beta = 8$ it is barely in agreement, just at the 99% CL. More constraints on the determination of the UT and a better determination of the QCD parameters will reduce the uncertainties in the determination of S from Eq. (48) and hence will help to further differentiate and possibly rule out some possibilities within the supersymmetric MFV scenario.

| m_H | m_q | m_{t_L} | m_{t_R} | m_{γ_1} | m_{γ_2} | $\tan \beta$ | S |
|-------|-------|-----------|-----------|----------------|----------------|--------------|------------------------|
| 115 | 880 | 400 | 150 | 170 | 189 | 5 | 2.56 0.08 |
| 175 | 880 | 400 | 150 | 170 | 189 | 5 | $2.52_{-0.06}^{+0.08}$ |
| 115 | 880 | 400 | 150 | 300 | 380 | 5 | 2.46 0.07 |
| 115 | 700 | 350 | 160 | 170 | 189 | 5 | 2.69 0.09 |
| 200 | 700 | 350 | 160 | 170 | 189 | 5 | 2.63 0.09 |
| 115 | 700 | 350 | 160 | 170 | 189 | 8 | 2.58 0.09 |
| 115 | 700 | 350 | 160 | 300 | 380 | 8 | 2.35 0.07 |

Table 1: Examples of input parameters to determine S , all the masses are expressed in GeV.

8 Conclusions

The goal of this note was to study the impact on the present limit on m_{B_s} on the determination of the unitary triangle (UT) parameters within the context of the SM and also to put bounds for certain classes of processes BSM for which the current UT analysis is useful. We have seen that the actual determination of the output value of $m_{B_s} = 19.96_{-1.01}^{+1.71}$ using the present limit on it ($m_{B_s} > 16.6$ ps⁻¹) agrees remarkably well with its output value without using m_{B_s} as a constraint: $m_{B_s} = 21.08_{-2.73}^{+2.83}$ and has 1% error in agreement with respect to the value obtained by the using the previous bound of $m_{B_s} > 14.5$ ps⁻¹, in this case $m_{B_s} = 19.18_{-1.35}^{+1.84}$. Even when the change in some of the parameters of the UT analysis is not drastic in comparison to previous determinations of them using the $m_{B_s} > 14.5$ ps⁻¹ and other sets of input data and analyses, [36]–[37], we found interesting to emphasize the importance on the CKM UT analyses of the determination of m_{B_s} and how this can be translated in tests of theories BSM.

The definitive measurement on m_{B_s} will provide indeed a good opportunity to test the consistency between the CP conserving processes – $\mathcal{V}_{ub} \neq \mathcal{V}_{cb}$, m_{B_d} and $m_{B_d} = m_{B_s}$ { and the CP violating ones { κ and $\sin(2\beta)$ {, since as we have seen with the present bound on m_{B_s} and the used set of experimental information, there is a slight disagreement between the resulting value for $\sin(2\beta)$ considering just CP conserving processes, which in this case renders a value of $\sin 2\beta_{CP\text{ conserv.}} = (0.751; 0.841)$, and the experimental reported value of $\sin 2\beta_{exp} = (0.623; 0.751)$, both intervals at 95% CL. An interesting possibility is that there is a beyond the SM (BSM) contribution to $\sin 2\beta$ such that we can express $\sin 2\beta = \sin(2\beta_{SM} + \beta_{B_d})$. We have seen this is possible taking into account the results for this phase as a consequence of allowing for $r_{B_d} e^{2\beta_{B_d}} = h B_{d,s}^0 \mathcal{H}_{eff}^{\text{Total}} \bar{B}_{d,s}^0 i = B_{d,s} \mathcal{H}_{eff}^{\text{SM}} \bar{B}_{d,s} i$ and the results of Eq. (45) which gives as an output $\beta_{B_d} = (-4.2; 1.23)^\circ$ and $r_{B_d} = 1.095 \pm 0.315 \pm 0.173$, both at the 68% CL.

Theories satisfying the minimal flavour violating (MFV) conditions, for which $\mathcal{V}_{ub} \neq \mathcal{V}_{cb}$ and $m_{B_d} = m_{B_s}$, used for the unitary triangle fits in the SM remain in the same form, can currently be tested at the same level of precision at which the anal-

yses in the SM are carried out. In particular a supersymmetric version of the MFV scenario where the first two generations of s-quarks are taken to be heavy and degenerate, allowing just for the contribution of the third generation, \tilde{t}_R and \tilde{t}_L can be tested in more detail since the change at the QCD NLO it is known [28]. We have tested this possibility for some samples of supersymmetric spectra, finding that although there is an agreement with most part of the possible range of the supersymmetric spectra, some regions are not favorable to an agreement between this and the output of the analyses of the experimental information. Indeed a measurement of m_{B_s} (and a better determination of \mathcal{Y}_{ub} and \mathcal{Y}_{cb}) will help to narrow the uncertainties in all the parameters related to it in the UT analysis, specifically the parameters related to observations BSM and hence helping us to disentangle more possibilities in this respect.

Acknowledgments

I would like to thank N. Leonardo for his early collaboration in this work, for discussions and for reading of the manuscript, I thank F. Krauss for the clarification of the notation of his work in hep-ph/9807238 and M. Voloshin for discussions. I also take here the opportunity to deeply thank A. Stocchi for help understanding the bayesian approach when I was developing the code for the determination of the CKM parameters. My work is supported in part by the DOE grant DE-FG 02-94ER .

A Experimental Inputs

| Fixed Parameters | | | | |
|------------------|----------|------------------------|----------------------|---|
| Parameter | Value | | Reference | |
| G_F | 1.16639 | 10^{-5}GeV^2 | [30] | |
| M_W | (80.425 | $0.038) \text{GeV}$ | " | |
| f_K | (0.1598 | $0.0015) \text{GeV}$ | \ | |
| m_K | (0.49765 | $0.00002) \text{GeV}$ | \ | |
| m_K | (3.4606 | $0.006) \text{GeV}$ | 10^{15}GeV | \ |
| $j_K j$ | (2.280 | $0.017) \text{GeV}$ | 10^{-3} | \ |
| $\tau\tau$ | (0.574 | $0.004)$ | [34] | |
| m_{B_d} | (5.2794 | $0.0005) \text{GeV}$ | [30] | |
| m_{B_s} | 0.55 | 0.007 | \ | |
| m_{B_s} | (5.375 | $0.0024) \text{GeV}$ | \ | |

Table 2: Input values of fixed parameters.

| Fitted Parameters | | | | |
|--------------------------|---|-----------------|------------------|-----------------|
| Parameter | Value | Gaussian errors | Flat errors | Reference |
| $j_{cb} j(\text{incl.})$ | (41.6 | 0.7) | 10^{-3} | [29] |
| $j_{cb} j(\text{excl.})$ | (41.3 | 1.0) | 10^{-3} | 1.8 10^{-3} \ |
| $j_{ub} j(\text{incl.})$ | (43.9 | 2.0) | 10^{-4} | 2.7 10^{-4} \ |
| $j_{ub} j(\text{excl.})$ | (38.0 | 2.7) | 10^{-4} | 4.7 10^{-4} \ |
| $j_{us} j$ | 0.2258 | 0.0014 | | \ |
| B_K | 0.79 | 0.04 | 0.09 | [30] |
| \overline{m}_c | (1.3 | 0.1) | GeV | " |
| \overline{m}_t | (161.5 | 3.0) | GeV | [32]* |
| α | 1.38 | 0.53 | | [33] |
| α_t | 0.47 | 0.04 | | [34] |
| $\sin 2\theta$ | 0.687 | 0.032 | | [30] |
| $m_{\overline{B}_d}$ | (0.506 | 0.005) | ps^{-1} | [31] |
| f_{B_s} | (0.276 | 0.038) | GeV | [38] |
| m_{B_s} | 1.24 | 0.04 | 0.06 | [35] |
| m_{B_s} | amplitude scan | | | [30] |
| | $(> 16.6 \text{ps}^{-1} \text{ at } 95\% \text{ C.L.})$ | | | |

Table 3: Input values of the fitted parameters. Taken from [32] and calculated at the pole.

B Tables of outputs

| Outputs | | | | |
|--|--|--|--|---------------|
| Parameter | Pre-Run II | No m_{B_s} | Post-Run II | |
| m_{B_s} [ps ⁻¹] | 0.212 _{-0.034} ^{0.032} | 0.238 _{-0.034} ^{0.032} | 0.222 _{-0.031} ^{0.035} | |
| $\mathcal{Y}_{ub} \neq \mathcal{Y}_{cb}$ | 0.358 _{-0.028} ^{0.026} | 0.345 _{-0.025} ^{0.024} | 0.353 _{-0.033} ^{0.030} | |
| $\sin 2$ | 19.18 _{-1.35} ^{1.84} | 21.08 _{-2.73} ^{2.83} | 19.96 _{-1.70} ^{1.71} | |
| \mathcal{P} | 98.90 _{-4.60} ^{4.29} | 102.98 _{-7.35} ^{6.47} | 100.55 _{-4.92} ^{3.98} | \mathcal{P} |
| R_b | 59.39 _{-5.07} ^{3.85} | 55.32 _{-5.39} ^{5.70} | 57.76 _{-4.72} ^{3.22} | |
| R_t | 0.419 _{-0.013} ^{0.008} | 0.421 _{-0.020} ^{0.016} | 0.419 _{-0.013} ^{0.011} | |
| $B_K q$ | 0.764 _{-0.044} ^{0.046} | 0.786 _{-0.047} ^{0.04} | 0.771 _{-0.055} ^{0.055} | |
| $f_{B_d} B_{B_d}$ [GeV] | 0.226 _{-0.014} ^{0.016} | 0.234 _{-0.016} ^{0.017} | 0.229 _{-0.026} ^{0.028} | |

Table 4: Output values of the fitted parameters. The three columns correspond respectively to the complete Classic Fit for the pre-run II fit, the fit without using m_{B_s} as a constraint and to the post-run II fit.

| Outputs | | | | | | |
|-------------------------------|--|--|--|-----------------|--|-----------------|
| Parameter | (i) | (ii) | (iii) | | | |
| m_{B_s} [ps ⁻¹] | 0.205 _{-0.052} ^{0.040} | 0.236 _{-0.042} ^{0.048} | 0.281 _{-0.059} ^{0.010} | | | |
| \mathcal{Y}_{ub} | (3.66 0.1) | 10 ³ | (4.9 0.05) | 10 ³ | (3.85 0.1) | 10 ³ |
| \mathcal{Y}_{cb} | (4.37 0.04) | 10 ² | (4.30 0.03) | 10 ² | (4.47 0.03) | 10 ² |
| m_{B_d} [ps ⁻¹] | 0.500 _{-0.099} ^{0.123} | 0.497 _{-0.023} ^{0.047} | 0.494 _{-0.021} ^{0.044} | | | |
| \mathcal{P} | (2.45 _{-0.37} ^{0.42}) | 10 ³ | (2.29 _{-0.154} ^{0.136}) | 10 ³ | (1.97 _{-0.32} ^{0.56}) | 10 ³ |
| $\sin 2$ | 0.764 _{-0.021} ^{0.018} | 0.756 _{-0.020} ^{0.019} | 0.764 _{-0.017} ^{0.016} | | | |
| R_b | 97.92 _{-8.52} ^{8.22} | 102.64 _{-8.76} ^{8.04} | 114.04 _{-6.25} ^{9.57} | \mathcal{P} | | |
| R_t | 60.38 _{-8.05} ^{7.68} | 55.67 _{-7.80} ^{7.08} | 47.82 _{-1.76} ^{11.13} | | | |
| $B_K q$ | 0.420 _{-0.021} ^{0.018} | 0.421 _{-0.019} ^{0.014} | 0.424 _{-0.012} ^{0.009} | | | |
| $f_{B_d} B_{B_d}$ [GeV] | 0.225 _{-0.016} ^{0.017} | 0.238 _{-0.016} ^{0.019} | 0.243 _{-0.024} ^{0.024} | | | |

Table 5: Output values of the fitted parameters. The three columns correspond to the three cases presented in Section (7.3.2): (i) Using the constraints $\mathcal{Y}_{ub} \neq \mathcal{Y}_{cb}$, $m_{B_s} = m_{B_d}$ and m_{B_d} ; (ii) $\mathcal{Y}_{ub} \neq \mathcal{Y}_{cb}$, $m_{B_s} = m_{B_d}$ and K and (iii) $\mathcal{Y}_{ub} \neq \mathcal{Y}_{cb}$, $\sin 2$ and $m_{B_s} = m_{B_d}$.

References

- [1] HFAG : B Lifetime and Oscillation Working Group: Results after the summer and fall 2005 conferences: <http://www.slac.stanford.edu/xorg/hfag/osc/december2005/index.html>
- [2] B. Aubert [BABAR Collaboration], arXiv:hep-ex/0602006.
- [3] <http://ckm.tter.in2p3.fr/>
- [4] <http://ut.triumf.ca.infn.it/>
- [5] M. Ciuchini, G. D'Agostini, E. Franco, V. Lubicz, G. Martinelli, F. Parodi, P. Roudeau, A. Stocchi, JHEP 0107 (2001) 013 [arXiv:hep-ph/0012308]. F. Parodi, P. Roudeau and A. Stocchi, Nuovo Cim. A 112, 833 (1999) [arXiv:hep-ex/9903063].
- [6] A. Hocker, H. Lacker, S. Laplace, F. Le Diberder, Eur. Phys. J. C 21 (2001) 225 [hep-ph/0104062].
- [7] A. Ali, D. London, Eur. Phys. J. C 18 (2001) 665; S. Melle, Phys. Rev. D 59 (1999) 113011; D. Atwood, A. Soni, Phys. Lett. B 508 (2001) 17.
- [8] Y. Grossman, Y. Nir, S. Plaszczynski, M. -H. Schune, Nucl. Phys. B 511 (1998) 69; S. Plaszczynski, M. -H. Schune [hep-ph/9911280].
- [9] <http://www.slac.stanford.edu/xorg/hfag/>
- [10] H. -G. Møller, A. Roussarie, Mathematical methods for $B^0\bar{B}^0$ oscillation analysis, Nucl. Instr. and Methods A 384 (1997) 491.
- [11] S. Laplace, Z. Ligeti, Y. Nir and G. Perez, Phys. Rev. D 65, 094040 (2002) [arXiv:hep-ph/0202010].
- [12] S. Bertolini, F. Borzumati, A. Masiero and G. Ridol, Nucl. Phys. B 353, 591 (1991).
- [13] G. D' Ambrosio, G. F. Giudice, G. Isidori and A. Strumia, Nucl. Phys. B 645, 155 (2002) [arXiv:hep-ph/0207036].
- [14] T. Inami and C. S. Lim, Prog. Theor. Phys. 65, 297 (1981) [Erratum -ibid. 65, 1772 (1981)].
- [15] M. Ciuchini et al.,
- [16] T. Goto, Y. Okada, Y. Shimizu and M. Tanaka, Phys. Rev. D 55, 4273 (1997) [Erratum -ibid. D 66, 019901 (2002)] [arXiv:hep-ph/9609512]. JHEP 0107, 013 (2001) [arXiv:hep-ph/0012308].

[17] K. A. Olive, M. Pospelov, A. Ritz and Y. Santoso, Phys. Rev. D 72 (2005) 075001 [[arX iv:hep-ph/0506106](https://arxiv.org/abs/hep-ph/0506106)].

[18] T. Goto, Y. Y. Keum, T. Nishi, Y. Okada and Y. Shimizu, Phys. Lett. B 460, 333 (1999) [[arX iv:hep-ph/9812369](https://arxiv.org/abs/hep-ph/9812369)].

[19] T. Nishi, Prog. Theor. Phys. 98 (1997) 1157 [[arX iv:hep-ph/9707336](https://arxiv.org/abs/hep-ph/9707336)].

[20] T. Goto, T. Nishi and Y. Okada, Phys. Rev. D 53, 5233 (1996) [Erratum -ibid. D 54, 5904 (1996)] [[arX iv:hep-ph/9510286](https://arxiv.org/abs/hep-ph/9510286)].

[21] T. Goto, Y. Okada and Y. Shimizu, Phys. Rev. D 58, 094006 (1998) [[arX iv:hep-ph/9804294](https://arxiv.org/abs/hep-ph/9804294)].

[22] A. Ali and D. London, Eur. Phys. J. C 9, 687 (1999) [[arX iv:hep-ph/9903535](https://arxiv.org/abs/hep-ph/9903535)].

[23] Bonn 2005eu S. Baek and P. Ko, Phys. Rev. Lett. 83, 488 (1999) [[arX iv:hep-ph/9812229](https://arxiv.org/abs/hep-ph/9812229)].

[24] D. Chang, W. Y. Keung and A. Pilaftsis, Phys. Rev. Lett. 82, 900 (1999) [Erratum -ibid. 83, 3972 (1999)] [[arX iv:hep-ph/9811202](https://arxiv.org/abs/hep-ph/9811202)].

[25] G. C. Branco, G. C. Cho, Y. Kizukuri and N. Oshimo, Phys. Lett. B 337, 316 (1994) [[arX iv:hep-ph/9408229](https://arxiv.org/abs/hep-ph/9408229)].

[26] M. Ciuchini, G. Degrassi, P. Gambino and G. F. Giudice, Nucl. Phys. B 534, 3 (1998) [[arX iv:hep-ph/9806308](https://arxiv.org/abs/hep-ph/9806308)].

[27] M. Dine and A.E. Nelson, Phys. Rev. D 48 (1993) 1277; M. Dine, A.E. Nelson and Y. Shimizu, Phys. Rev. D 51 (1995) 1362; M. Dine, A.E. Nelson, Y. Nir and Y. Shimizu, Phys. Rev. D 53 (1996) 2658.

[28] F. Krauss and G. So, Nucl. Phys. B 633, 237 (2002) [[arX iv:hep-ph/9807238](https://arxiv.org/abs/hep-ph/9807238)].

[29] J. Alexander et al. [Heavy Flavor Averaging Group (HFAG)], [arX iv:hep-ex/0412073](https://arxiv.org/abs/hep-ex/0412073).

[30] S. Eidelman et al. [Particle Data Group], Phys. Lett. B 592, 1 (2004).

[31] <http://www.slac.stanford.edu/xorg/hfag/osc/december2005/index.html>

[32] <http://www-cdf.fnal.gov/physics/new/top/top.html>

[33] A. J. Buras, M. Jamin and P. H. Weisz, Nucl. Phys. B 347, 491 (1990).

[34] S. Herrlich and U. Nierste, Nucl. Phys. B 419, 292 (1994) [[arX iv:hep-ph/9310311](https://arxiv.org/abs/hep-ph/9310311)].
 G. Buchalla, A. J. Buras and M. E. Lautenbacher, Rev. Mod. Phys. 68, 1125 (1996) [[arX iv:hep-ph/9512380](https://arxiv.org/abs/hep-ph/9512380)].

[35] M. Battaglia et al., arXiv:hep-ph/0304132.

[36] J. Charles et al. [CKM fitter Group], Eur. Phys. J. C 41, 1 (2005) [arXiv:hep-ph/0406184].

[37] M. Bona et al. [UT fit Collaboration], arXiv:hep-ph/0509219.

[38] M. Bona et al. [UT fit Collaboration], JHEP 0507, 028 (2005) [arXiv:hep-ph/0501199].

[39] F. Gabbiani, E. Gabrielli, A. Masiero and L. Silvestrini, Nucl. Phys. B 477, 321 (1996) [arXiv:hep-ph/9604387].

[40] R. Barbieri, L.J. Hall and A. Romanino, Nucl. Phys. B 551, 93 (1999) [arXiv:hep-ph/9812384].

[41] R. G. Roberts, A. Romanino, G. G. Ross and L. Velasco-Sevilla, Nucl. Phys. B 615, 358 (2001) [arXiv:hep-ph/0104088].

[42] G. G. Ross, L. Velasco-Sevilla and O. Vives, Nucl. Phys. B 692, 50 (2004) [arXiv:hep-ph/0401064].